# UNIVERSITY OF GENOA

## MASTER'S PROGRAM IN BIOENGINEERING

Thesis submitted in partial fulfillment of the requirements for the title of

Master of Bioengineering

# The role of electroosmosis during PEF application in plant and animal tissues from the perspective of mechanical and electrical evaluation

Enrico Sidoti

29th March 2023

*Thesis advisor:*        Prof. Laura Pastorino, Prof. Samo Mahnic-Kalamiza

# Contents

# Abstract

Electroporation is an electrical phenomenon in which biological samples subjected to a sufficiently high electric field temporarily increase permeability and conductivity. This phenomenon is used in various fields, including the biomedical or food processing fields. Electroosmosis, on the other hand, is a mass transport process that allows the movement of a liquid subjected to the action of an electric field, relative to a stationary solid with electrically charged walls, due to the interaction between charge redistribution and the electric field. This effect often occurs in conjunction with other electrical phenomena and also has various applications in civil engineering, biomedical engineering and food processing.

Continuing the work carried out at the Ljubljana biocybernetic laboratory by Genovese, the mass transport phenomena resulting from electroosmotic flow following electroporation were observed and studied. Therefore, a system was devised to detect electroosmotic flow by subjecting a biological sample to a compressive force via a texture analyser, on which a train of 8 high-voltage pulses was released via an HV generator in order to electroporate the system.

The mechanical data were acquired using the software inside the texture analyser, while the electrical data were acquired using an oscilloscope. Subsequently, these data were analysed using the MATLAB environment.

Samples in which electroosmotic flow was induced via an LV generator following a standard application of electroporation were also analysed.

Electroosmotic flux was found to be detectable in both plant and animal tissue (whose data were made available by Genovese et al.), albeit to a modest extent. Plant tissue presents greater difficulties in the detection of flux using this acquisition method. It has also been shown that electroosmotic flux is significantly higher when the sample is previously treated by electroosmosis.

# Chapter 1

# Introduction

## 1. Introduction

### 1.1. The electroporation phenomenon

Electroporation is an electrical phenomenon which can occur if a biological material (cell, tissue) is exposed to a sufficiently high electric field, which is delivered by applying high-voltage electrical pulses.

Almost every cell presents an electric potential difference on the plasma membrane, called the resting transmembrane voltage, due to the differences in chemical composition (ionic imbalance) between the internal and the external part of the cell, generated and regulated by a system of ion pumps and channels in the membrane. The cell's exposure to the externally applied electric field adds a component to the resting transmembrane voltage, resulting in structural changes to the membrane itself. This process increases membrane permeability and conductivity [Kotnik et al., 2019].

The strength of the electric field and the exposure time influence the effect of the electroporation, in fact, if these two parameters are below a certain threshold, this phenomenon does not occur, conversely, if the transmembrane voltage is sufficiently high, it is possible to observe electroporation.

Furthermore, once a certain transmembrane voltage is exceeded, depending on the intensity of the electric field and the duration of the exposure time, the phenomenon can be reversible [Granot and Rubinsky 2008] or irreversible [Geboers et al. 2020].

The former (reversible) case occurs when the electric field and time of exposure are above the electroporation threshold, causing the membrane conductivity and permeability to increase only temporarily, and after the end of the externally applied electric field, the biological material is able to return to its original state (the cell activates repair mechanisms

and re-establishes homeostasis). On the other hand, irreversible electroporation involves an electric field and exposure time above the irreversible electroporation threshold, leading to a permanent loss of cell homeostasis, eventually leading to cell death. Although both reversible and irreversible electroporation involve the same phenomenon, i.e. electroporation, differing only in intensity, the end result (cell recovering or dying) allows for different applications in many fields, such as environmental science [Huo et al. 2022], biomedicine [Sersa et al. 2008], food processing [Dymek. 2015], and biotechnology [Kotnik et al. 2015].

## *1.1.1.     Food processing applications*

In the food industry, alternative technologies have been investigated to improve food quality and optimize food processing while reducing energy consumption, and pre-treatment of food by electroporation has been identified as a potential technology to achieve these goals.

Since the application of electroporation induces a higher level of cell membrane permeability, which means a reduction of resistance to mass transfer, it can be used as a pre-treatment to increase the yield in the production of fruit juices [Mahnič-Kalamiza et al. 2014], to improve the drying operations by modifying the speed of transfer of water [Sack et al. 2008], and to enhance the extraction of valuable compounds from the cells [Parniakov et al. 2016].

Electroporation can also be used for cryopreservation. Freezing is a common technique of food preservation, but formation of crystals may alter food characteristics such as flavour and texture. For this reason, cryoprotectants, i.e. substances which prevent the formation of crystals caused by freezing, are used and introduced into the cells in two different ways: via osmotic dehydration [Moraga et al. 2006] in a hypertonic solution, or by vacuum impregnation [Velickova et al. 2013]. The effect of combined electroporation and cryoprotectant impregnation was studied on spinach leaves [Dymek et al. 2015] to observe how their properties might be altered by the process. The cell membrane of spinach has low permeability without pre-treatment, so cryoprotectants are unable to reach the interior of the cell. Treatment of spinach leaves with reversible electroporation enabled frozen and subsequently thawed spinach leaves to retain their texture and flavour, as the cells remained alive even after thawing.

## *1.1.2. Biomedical applications*

Electroporation has been used for the first time in the biomedical field by Neumann and his colleagues in 1982 [Neumann et al. 1982] for a gene-transfer technique called gene electrotransfer. This technique involves the use of plasmid DNA (pDNA), which is an excellent option as it removes the need for a biological vector, increasing the safety of the process compared to a viral vector system. Were the electroporation process not applied, the delivery system for pDNA across the cell membrane would be inefficient with a low level of subsequent gene expression. Electroporation therefore solves this problem by improving delivery and gene expression by increasing the permeability of the cell membrane. So, in their work Neumann et al. used pulsed electric fields *in vitro* in order to permeabilize the cell membrane and deliver foreign DNA into mouse cells. Once the cell is permeabilized, the DNA can move towards the electrodes because of a phenomenon called electrophoresis: an electrokinetic mechanism where electrically charged colloidal particles or ionic macromolecules, can move under the influence of an electric field. If the particles (colloidal particles, or ions) are positively charged, they will move towards the cathode, otherwise, they will move towards the anode. Following the Neumann et al. study, DNA electrotransfer has been investigated in several tissues [Trezise 2002; André et al. 2008; Hargrave et al. 2014], with promising applications of gene electrotransfer for tumour cells, where the extracellular matrix can hinder the migration of DNA in the extracellular space, thereby increasing the difficulty of transport of pDNA into the cell [Cemazar et al. 2012]. The property of gene electrotransfer to be highly efficient and to have few adverse effects has promoted its use as a nonviral method of gene delivery. Although plasmid transport has been shown to be highly efficient in various tissues, clinical trials of the use of gene electrotransfer have been conducted mainly in muscle, skin, and tumours [Heller and Heller 2015].

Electroporation has also been studied as a tool for introducing membrane-impermeant drugs to kill cancerous cells, this process is called electrochemotherapy [Okino and Mohri 1987; Hofmann et al. 1999; Miklavčič et al. 2014; Geboers et al. 2020]. Chemotherapy

involves the use of drugs that target dividing cells but also attack normal tissues, which can have some side effects. More specifically, these drugs target the intracellular material of cells whose membrane in the normal homeostatic state has low permeability. Therefore, in order to increase the effectiveness of chemotherapy, larger concentrations of drugs are required, consequently increasing side effects. Electroporation, by increasing the permeability of the cell membrane, allows the quantity of injected drugs to be reduced, and the side effects to be decreased.

Another method to treat tumour cells is the nonthermal tissue ablation [Davalos et al. 2005], a technique which involves irreversible electroporation. By applying an electric field, one of the biophysical effects which occurs is Joule Heating. Heating causes cell death in the target volume, which also includes blood vessels and extracellular matrix. Devalos et al. proposed a protocol to get the irreversible electroporation with minimal thermal damage [Edd et al. 2006] that is fast and simple to apply, since only the insertion of needle electrode is needed.

By means of this short review of numerous electroporation applications we intend to demonstrate the importance of the technique and technology of electroporation to biomedicine, and thus highlight the importance of us understanding the basic mechanisms of the phenomenon and accompanying processes such as mass transfer processed in great detail.

## *Biomedical applications where electrokinetic mechanisms of transport are of importance*

Electrokinetic mechanisms that enable mass transport have proven to be an important resource in the biomedical field, as various medical techniques based on them have been studied and developed. DNA electrophoresis comes to mind as perhaps the best known example. Another example is the combination of electroporation and electrolysis (also known as "electrolytic ablation", shortened to "E2") for tissue ablation [Klein et al. 2017]. Electrolysis is a process where electrical energy is converted into chemical energy, causing non-spontaneous reactions. The products of these reactions, among other, are usually positively and negatively charged ionic species. The technique of electrolytic ablation uses, instead of square pulses (as used in electroporation), an exponentially decaying pulse,

which is composed of two stages. The beginning of the pulse is considered to be a "high voltage" stage, supposed to increase the permeability of the cell membrane, while the latter part of the pulse (its tail end) is considered a "low voltage" stage, and since, through the nature of the exponentially decaying pulse, it is longer than the high voltage stage, this low voltage part is supposed to deliver enough electric charge to cause an electrolytic process at the interface of the electrode [Klein et al. 2020]. Various chemical species are then formed near the electrodes and diffuse due to a difference in electrochemical potential. The consequence of this process is a pH change in the medium (which can be tissue) leading to an acidic region (low pH) at the anode, and a basic (alkaline) region of high pH at the cathode [Phillips et al. 2015]. Since cells, especially electroporated cells, are sensitive to low and high pH values, these changes in pH can be fatal to the cells. Usually, the technique of tissue ablation is achieved by irreversible electroporation, as it can lead to immediate necrosis of a tissue exposed to an electric field, which allows ablation of a significant volume of tissue. In the E2 technique, despite the use of reversible electroporation, the synergy between electrolysis and electroporation improves tissue ablation, resulting in tissue ablation areas comparable to those achieved by irreversible electroporation in a shorter time.

Another example could be the electrokinetic convection-enhanced delivery of solutes to the brain [Faraji et al. 2020]. In medicine, the pressure-induced convection is useful to deliver substances in brain areas which need gene therapy or in an area where there are deep and difficult to remove tumours. The limit of this method is the low level of control of the flow, and neurological damage may happen because of neural distortion. By applying an electric field, electrokinetic convection-enhanced delivery has been demonstrated in laboratory. Since the flow follows the electrical current, this technique provides more control than the alternative/conventional technique, and a lower pressure is required.

Also, it has been proposed that tumor tissue could be treated with electrolysis combined with an electrokinetic mechanism of transport called electroosmosis [Vijh 1999a] that will be explained in the next section.
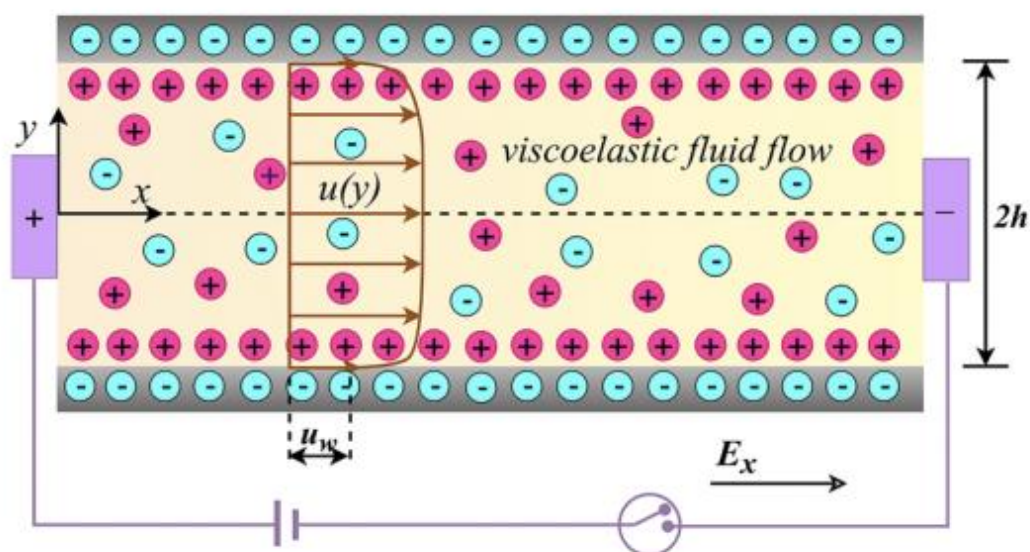
## 1.2.  Electroosmosis and its applications



Figure 1: example of electroosmotic flow

The term electroosmosis or electroendosmosis indicates the motion of a fluid, usually water, under the action of an electric field, which occurs in porous materials. In the interphase between a solid layer and an electrolytic solution, an electric double layer always exists due to the selective adsorption of ions or through charge formation by ionization of groups in the surface of the solid itself. Electroosmosis is often an accompanying process to other processes such as electrophoresis [Faraji et al. 2020], or is the primary mechanism of desired mass transport, such as when applied for the electrochemical treatment of tumours [Vijh 1999a].

Electroosmosis has been discovered in 1949 [Casagrande 1949] as a useful technique to improve waterlogged clayey soils, then it found many applications in the civil engineering field [Gray and Mitchell 1967] due to its effectiveness in fine-grained and low-permeability materials such as silts and clays. One of the solved problems thanks to electroosmosis is the mould in houses or buildings in general, which is a serious problem that cannot be overlooked: it is not just an aesthetic problem, but is a health danger for those most at risk such as children, the elderly, and those suffering from respiratory diseases such as asthma. Electroosmosis in bentonite clay was studied thoroughly [Iwata et al. 1991] using the Kobayashi equation and a system which consisted of a piston in a way to compress the

10

material and reduce its void ratio. This study has also shown differences between the two electrodes: due to the electroosmosis phenomenon, since the water flows in the anode-to-cathode direction, consequently the cathode becomes wet, while the anode becomes dry. However, the civil engineering is not the only field where electroosmosis has been applied. In food engineering, for example, it has also been demonstrated [Menon et al. 2019] that the electroosmotic dewatering could present an energy efficient technique for drying of food materials. In their paper, Menon et al. have shown the advantages of the electroosmosis process with respect to classical thermal processes: electroosmosis-assisted dewatering has a lower energy consumption than the thermal process, and is convenient from an economical and environmental perspective. From a biomedical point of view, electroosmosis is relevant since it is involved in many applications. Vijh, in his work [Vijh 1999b; Vijh 1999a; Vijh 2004], has theoretically demonstrated the principles behind the efficacy of the process. A voltage of about 6-10 V with a current of 40-100 mA if applied for 1 or 2 hours on the tumour tissue would result in, due to the electrolysis process, the anode becoming strongly acidic, since it attracts positive ions, while the cathode would become strongly alkaline, since it attracts negative ions; by means of these extreme pH changes, proteins are denatured, and cell death occurs in the volume exposed to the electric field for a sufficient amount of time and with sufficient changes in pH. Concurrently, water flow from the anode to the cathode occurs, due to electroosmotic dewatering, which is proportional to the current or charge delivered. The water flow and the subsequential dehydration of tissue have been proposed as the main causes of death cell, helped by the presence of the strongly acidic medium at the anode and strongly alkaline medium at the cathode.

The electroosmotic process certainly has some limitations, e.g. the positioning of the electrodes during the electrochemical ablation of tissue is crucial, since it influences the direction of the flow, moreover, the treatment of large tumours due to sheer volume could be very challenging. It is perhaps due to this reason that electrochemical treatment of tumours is not a widely known, researched, or practiced procedure outside some very limited research studies.

# 1.3. Electrochemical reactions during application of PEF

Electrochemical reactions are not negligible during the application of electroporation or electroosmotic procedures. Several authors have addressed this issue, both in food processing in applications such as microbial inactivation or pasteurisation [Pataro et al. 2014], and in the biomedical field with applications such as gene electrotransfer [Marino et al. 2017]. In these application areas, the specified goal must be achieved with a minimum level of material contamination. In the case of food, contamination can lead to a loss of nutrients or flavour, in the biomedical field, it can introduce unwanted substances into tissue, and a change in pH can severely damage the cells/tissues. In most studies investigating toxicity in food applications, different solutions were used, mostly related to the optimisation of the treatment chamber. The treatment chamber system connected to the high-voltage generator acts like an electrolytic cell. As soon as current flows, a double layer is formed at the interface between the electrode and the solution, which acts like a capacitor. When these capacitors are charged, the current is purely capacitive due to the low voltage, so reactions such as oxidation and reduction are avoided. If, on the other hand, the voltage reaches a certain threshold, oxidation phenomena occur at the anode and reductions at the cathode. These redox reactions can cause different phenomena, as electrode fouling, electrode corrosion, and a metallic contamination of the treated medium. So, the corrosion is strictly connected to the deposition of material at the cathode and anode, and with electrode fouling may cause the electric field distortion, decreasing the efficiency of the treatment but also the shelf life of the electrode. Some example of reactions that may occur in cathode or anode are reported in [Merrill et al. 2005]:

- $2H_2O + 2e^- \rightarrow H_2 \uparrow + 2OH^-$       (reduction of water, cathode)
- $Fe^{3+} + e^- \leftrightarrow Fe^{2+}$       (simple electron transfer, cathode)
- $Cu^{2+} + 2e^- \leftrightarrow Cu$       (Cu metal deposition, cathode)
- $PtO + 2H^+ + 2e^- \leftrightarrow Pt + H_2O$       (Oxide formation and reduction, cathode)
- $IrO + 2H^+ + 2e^- \leftrightarrow Ir + H_2O$       (Oxide formation and reduction, cathode)

- $IrO_2 + 4H^+ + 4e^- \leftrightarrow Ir + H_2O$ (Oxide formation and reduction, cathode)

- $2IrO2 + 2H^+ + 2e^- \leftrightarrow Ir_2O_3 + H_2O$ (Oxide formation and reduction, cathode)

- $Pt + H^+ + e^- \leftrightarrow Pt - H$ (Hydrogen atom plating, cathode)

- $2H_2O \rightarrow O_2 \uparrow + 4H^+ + 4e^-$ (Oxidation of water, anode)

- $Pt + 4Cl^- \rightarrow [PtCl_4]^{2-} + 2e^-$ (Corrosion, anode)

- $2Cl^- \rightarrow Cl_2 \uparrow + 2e^-$ (Gas evolution, anode)

- $Fe \rightarrow Fe^{2+} + 2e^-$ (Anodic dissolution, anode)

- $2Ag + 2OH^- \leftrightarrow Ag_2O + H_2O + 2e^-$ (Oxide dissolution, anode)

Not all these reactions occur during a process, as they vary according to the electrode, but also to the material subjected to the treatment. The use of chlorine-free tissue or solutions is suggested because studies have shown the formation of toxic reactions for the material itself at the electrode level. In fact, chlorine can increase the metal release from the electrode, due to the oxidation reaction at the anode [Pataro et al. 2014].

In biomedical applications, most of the above chemical reactions can take place provided that stainless (or medical) steel electrodes are used for electric field and current delivery. The biological tissue does have some pH buffering capabilities, but these are of course finite, and at some point of treatment intensity (sufficient charge exchanged between the electrodes and tissue), adverse electrochemical effects will become important. It is therefore imperative that potential risks and hazards are well known in advance, and that researchers are aware of mass transfer processes such as electrophoresis and electroosmosis that will contribute to the migration of harmful substances through the tissue due to electric field effects.

# 1.4.  The Dual porosity model

Describing mechanical properties of biological materials is much more complex than of mineral-based materials. Cell structure itself is complex, intra- and extracellular media have different properties, so the flow of the liquid will behave differently in one or the other medium. In addition, plant tissue and animal tissue differ in structure, since plant tissue presents with a cell wall, a component which is missing in the animal tissue. This component of the cell gives a more solid structure to the cell and add a level of complexity (and porosity) in plant tissues that is absent in animal tissues.

To achieve the aim of this thesis, it was necessary to carry out experiments that required the application of the electroporation process on a plant tissue subjected to a compressive force, since our aim was to detect the very small force resulting from electroosmosis. As pressing is an important industrial operation for the extraction of liquids or juices, it has been extensively studied and modelled over the years. Lanoiselle et al. [Lanoisellé et al. 1996], for example, studied and modelled the process of pressure extraction from plant tissue. Subsequently, based on this work, a further model was proposed, which includes the process of electroporation during pressure from biological tissue: the dual porosity model [Mahnič-Kalamiza and Vorobiev 2014]. This model considers separately the porosity of the intracellular space and the porosity of the extracellular space in every specific tissue and provides a theoretical approach to describe the effects of electroporation on cell membrane hydraulic permeability. A comparison of the proposed model with experimental data derived from the pressure of cylindrical sugarbeet sample was presented to show how the model may be used in practice to explain empirically reported kinetics. Then, using this theoretical model as a guide, an experimental setup was created to accomplish the thesis's suggested purpose.

The experiment that was carried out in the 2014 study of Mahnič-Kalamiza and Vorobiev is illustrated in Figure 2 below, and is in many aspects identical to the experiments performed within the scope of this work.
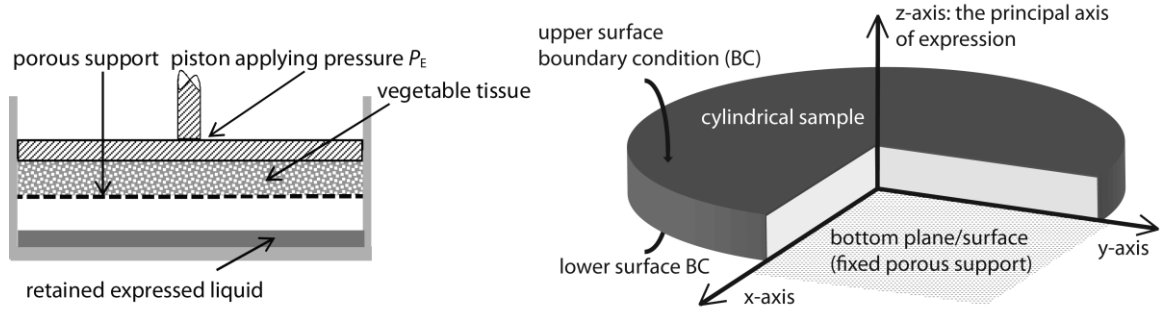
Figure 2: The pressing experiment and reference coordinate system from the perspective of the tissue sample. Reproduced from [Mahnič-Kalamiza and Vorobiev 2014] with the author's permission.

The dual porosity model for the expression of liquid from biological (plant) tissue postulates two liquid pressures – that of the intracellular space (or medium) and that of the extracellular space (or medium). The differential equations for the pressing experiment as illustrated in Figure 2 were found to be

$$\frac{1}{G_{\varepsilon,e}}\frac{\partial p_e}{\partial t} - \frac{\partial}{\partial z}\left(\frac{k_e}{\mu}\frac{\partial p_e}{\partial z}\right) - \frac{\alpha}{\mu}\left(p_i - p_e\right) = 0 \tag{1}$$

$$\frac{1}{G_{\varepsilon,i}}\frac{\partial p_i}{\partial t} + \frac{\alpha}{\mu}\left(p_i - p_e\right) = 0 \tag{2}$$

The initial and boundary conditions for eq. 1–2 are

$$p_{e0} = p_{e0}(z,0) = p_{i0} = p_{i0}(z,0) = P_E \tag{3}$$

$$p_e\big|_{z=0} = 0 \tag{4}$$

$$p_i\big|_{z=0} = p_{i0}e^{-\frac{\alpha G_{\varepsilon,i}}{\mu}t} \tag{5}$$

$$\frac{\partial p_e}{\partial z}\bigg|_{z=h} = \frac{\partial p_i}{\partial z}\bigg|_{z=h} = 0 \tag{6}$$

In the above equations, $p$ denotes liquid pressure, $t$ time, $z$ is the spatial coordinate along the axis of pressure application, indices 'e' and 'i' denote extracellular and intracellular space, respectively, while $\alpha$, $\eta$, and $G$ are material constants related to either the porosity, compressibility, or hydraulic permeability of the tissue, and are not relevant for the purposes of this discussion. $P_E$ is the externally applied pressure (via the piston of the

texture analyzer) and is introduced into the system through the initial condition (eq. 3). It is interesting that the system of equations 1–6 has an analytical solution

$$p_i(z,t) = \frac{4p_{i0}}{\pi} \sum_{n=0}^{\infty} \frac{1}{2n+1} \left( C_1 e^{\gamma_{n,1} t} + C_2 e^{\gamma_{n,2} t} - e^{-\tau^{-1} t} \right) \sin\left( \frac{(2n+1)\pi}{2h} z \right) + p_{i0} e^{-\tau^{-1} t} \tag{7}$$

where

$$C_1 = \frac{\left( \dfrac{p_{e0}}{p_{i0}} - 1 \right) \tau^{-1} - \gamma_{n,2}}{\gamma_{n,1} - \gamma_{n,2}}, \tag{8}$$

$$C_2 = \frac{\left( 1 - \dfrac{p_{e0}}{p_{i0}} \right) \tau^{-1} + \gamma_{n,1}}{\gamma_{n,1} - \gamma_{n,2}} \tag{9}$$

and

$$\gamma_{n_{1,2}} = \frac{-\left( \tau^{-1}\delta + \lambda_n^2 v \right) \pm \sqrt{\left( \tau^{-1}\delta + \lambda_n^2 v \right)^2 - 4\lambda_n^2 v \tau^{-1}}}{2}, \tag{10}$$

where, for the sake of algebra, we have set

$$v = \frac{k_e G_{\varepsilon,e}}{\mu}; \quad \tau^{-1} = \frac{\alpha G_{\varepsilon,i}}{\mu}; \quad \delta = \left( 1 + \frac{G_{\varepsilon,e}}{G_{\varepsilon,i}} \right); \quad p_{i0} = p_i(z,0); \quad p_{e0} = p_e(z,0).$$

The eigenvalues $\lambda_n$ equal $\lambda_n = (2n+1)/2 \cdot \pi/h$ ($h$ is the height of the tissue sample).

For extracellular liquid pressure $p_e$, we have

$$p_e(z,t) = \frac{4p_{i0}}{\pi} \sum_{n=0}^{\infty} \frac{1}{2n+1} \left( \left( \gamma_{n,1}\tau + 1 \right) C_1 e^{\gamma_{n,1} t} + \left( \gamma_{n,2}\tau + 1 \right) C_2 e^{\gamma_{n,2} t} \right) \sin\left( \frac{(2n+1)\pi}{2h} z \right) \tag{11}$$

where all coefficients are calculated according to expressions already defined for intracellular pressure.

Now, the externally applied pressure $P_E$ is present in both solutions (for the extra- and the intracellular space) via means of the initial intracellular pressure $p_{i0}$ (see first term in eqs. 7 and 11). It is precisely here that the electroosmotic pressure we are interested in, $P_{EOS}$, i.e. the pressure exerted on the liquid in tissue due to the electric field imposed on the

tissue sample (and consequent electric current through the sample), couples as an additional pressure to the externally applied one in our dual porosity model. Thus, equation 3 could be rewritten, for the case when (and only if/when) electroosmosis is present, as

$$p_{e0} = p_{e0}(z, 0) = p_{i0} = p_{i0}(z, 0) = P_E + P_{EOS} \tag{12}$$

Equation 12 can be thought of as the fundamental theoretical equation behind all of the experiments carried out within the scope of this work. Equation 12 fundamentally expresses that during pulsed electric field (or DC field/current) application to the tissue, there will be a detectable additional pressure (to the already imposed pressure by the texture analyser) present that should be adding to the compaction (or countering it!) of the tissue sample that we measure as deformation by the texture analyser. Why or how could it be countering it? We also postulate that, since the direction of electroosmotic flow is, generally, from the anode (+) towards the cathode (-), the electroosmotic liquid pressure $P_{EOS}$ can have a positive or negative sign with respect to the $z$ axis (i.e. the axis of pressure application by the piston), depending on whether the anode is at the top of the tissue sample or at the bottom, and cathode of course vice-versa. We intend to confirm whether this theoretical model is valid via the performed experiments, the details of which are written out in the following sections.

# 1.5.  Thesis hypothesis and aims

This thesis can be considered a continuation of previous studies done by Genovese et al. [Genovese et al. 2021; Genovese et al. 2023]. They reported on studies employing pulsed electric fields as pre-treatment for food applications; the aim of their study was to investigate the degree of membrane permeabilization in animal and plant tissues (chicken, potato, and apple) exposed to various pulsed electric field protocols. Different assessment methods such as electrical impedance, current voltage measurements, and magnetic resonance imaging were used to evaluate degree of tissue permeabilization.

Pulsed electric fields are useful since they can be used to achieve a permeabilized state of the cell membrane, and consequently enhance mass transfer, by means of which we can, for instance, increase the release of sugars from cells or introduction of substances into cells which would otherwise not be able to or would only poorly permeate out of/into the cell. The focus in this study was on the mass transfer, in particular, mass transfer as resulting from electroosmosis.

For what concerns this thesis' aims, we were interested in studying mass transport in plant tissue with regards to the effect of electroporation and the extent of concurrent and subsequent electroosmosis. To see whether the effect is also present in animal tissues, we analysed compression curves obtained previously by Genovese et al. (scientific publication on the results of the study is in preparation).

We decided to predominantly use plant tissue, precisely potato tuber tissue, for reason of easier experimentation, availability of the material, and because of the high-water content as well as high electrical conductivity of this vegetable material. The water content is a fundamental requirement since either by electroporation or electroosmosis some water is supposed to be released, which we can detect/measure as described in the following Materials and Methods chapter. The electroporation allows to increase permeability and conductivity of the cell membrane, and the electroosmosis resulting from the electric field/current causes a redistribution of the intracellular liquid within the treated sample, i.e., the water released from the cells flows in the direction of the cathode.

The use of tissue from a plant with low water content (e.g., apple) would not allow the effects of these two processes to be evaluated clearly, as there would be, such is our theoretical assumption, negligible or barely detectable electroosmotic flow.

Starting from the theoretical basis established by the model of Mahnič-Kalamiza and Vorobiev [Mahnič-Kalamiza and Vorobiev 2014] (see preceding section on the dual porosity model), an experimental setup has been built. In order to record the effects of electroosmosis during and after electroporation, we used a cylindrical sample of potato tissue on a texture analyser (a machine capable of delivering a constant force by piston and precisely measuring the piston displacement), and carefully recorded the load (compressive force – kept constant), and the resulting sample deformation (via piston displacement).

The idea behind this method of acquisition is that by applying an appropriate voltage capable of causing electroporation in tissue, we expect to be able to detect, via the texture analyser, a force that would presumably superimpose to the compression imposed by the texture analyser; depending on the polarity of the electrodes, the superimposed pressure either counters the pressure of the texture analyser piston, or adds to it. Thus, the hypothesis is that the polarity and direction of the electroosmotic flow will either add to the compressive pressure of the texture analyser or counter it, resulting in a retarded or accelerated compression kinetics of the tissue sample. In other words, a force in the same direction of piston movement corresponds to greater compression; in the case of a force in the opposite direction, we expect to get less/a reduction in compression.

Two different generators were needed for the experiments: a high voltage (HV) generator to apply a train of short, high-voltage electroporation pulses, and a low voltage (LV) generator to apply a constant (DC) voltage and current for electroosmotic flow after electroporation.

This project has two different aims, initially we studied the electroosmosis during the application of electroporation pulses alone, to determine if electroosmosis is an important mass transfer mechanism during industrial treatment of food materials with pulsed electric fields, and then in the second part of the project we also observed the electroosmosis after the pulses using constant voltage and current (DC fields) to prove or disprove the hypothesis that electroosmotic flow results in a pressure that is superimposed to the pressure of the texture analyser and that the direction of the electroosmotic pressure depends on the chosen polarity of the electrodes.

One of the standard protocols used for electroporation consists of a train of 8 pulses, 100 $\mu$s each, delivered at a rate of 1 s$^{-1}$ [Marty et al. 2006] The delivery of high voltage can electroporate the exposed tissue, so the first objective is to determine if the electroosmotic process is detectable during electroporation pulse delivery using the aforementioned setup;

analysing the compression from the delivery of high voltage pulses for the duration of the trial, some effects of the additional force due to electroosmosis may be detected by the texture analyser and visible in so-called compression curves (see figures under chapter Results).

For the second objective, i.e., the study of electroosmosis following electroporation, the idea is to electroporate the membrane with a high-voltage generator, using the same protocol as in the first set of experiments, and then to use a low-voltage generator for a longer period of time in order to generate the electroosmotic flow. Since electroporation will increase the permeability of the membrane and cause water to leak out from the cells into the extracellular space, the LV generator will then allow for the application of a constant electric field and current, which results in the flowing of the water by electroosmosis. Using the texture analyser acquisition method, we wanted to determine a range of parameters within which the electroosmotic flow can be observed. Besides, we wanted to observe which electroporation parameters would best increase the electroosmotic flow. Finally, a comparison was made between samples treated with electroporation followed by electroosmosis and samples treated with electroporation or electroosmosis exclusively, to demonstrate conclusively the effect of electroosmosis on tissue consolidation kinetics and thus mass transport.

# Chapter 2

# Materials and methods

## 2. Materials and methods

The experiments were divided in two different protocols: the first one is a "standard" electroporation protocol (standard in the sense it was standardized in the scope of a clinical study on use of electroporation for electrochemotherapy) where the aim is to verify the presence of the electroosmotic flow only with the application of a train of HV pulses.

The second one allows us to evaluate the differences between a standard electroporation protocol and a protocol where an electroosmotic flow is induced using direct currents; a high voltage generator is used that enables us to first electroporate the cells in the tissue by delivering a train of HV pulses, and subsequently, a LV generator is switched on that enables us to deliver a constant current in order to induce a temporally more constant electroosmotic flow through the tissue.

The HV generator first permeabilises cell membranes, so that the fluid which was inside of the cells is liberated and can flow into the extracellular space, through which it is then transported due to a combination of contributing factors. One of these factors is turgor pressure loss, i.e., there is some expulsion of liquid from the sample purely through means of turgor pressure liberation (the sample after electroporation treatment becomes soft and much less turgid), and the second contributing factor would be the electroosmosis. The direction of the electroosmotic flow will depend on the polarity of the electric field/current, as per our hypothesis. A dehydration test preceded the experiments so as to determine the initial water content of the potato tuber tissues, making sure we were always working with material that was sufficiently high in water content and one batch of experimental material did not too significantly differ from another batch, which could influence our end results.

## 2.1. Dehydration test



Figure 3: potato sample

The dehydration test was necessary to establish the initial water content of the potato tuber tissue. Every plant has a different water content, and since the experiments expect a flow of the water in the tissue due to the electric current, it is recommended to choose a plant which has a high, but perhaps more importantly, a consistent level of water content.

For this test, twelve aluminium cups and twelve samples of potato cut into cylinders of 6 mm thickness and 25 mm in diameter were used (Figure 3). First of all, the aluminium foil cups were numbered and weighed, and subsequently, a sample of plant tissue was added to each aluminium cup and weighed again. Once the samples were weighed, they were placed in the aluminium foil cups in an oven at 70 degrees Celsius for 72 hours.

After this time, the samples were weighed again.

The calculation using the weight of the lost humidity showed that the water content in fresh tissue was around 82 %, which is a reasonable figure considering the degree of freshness of the potato (store-bought, cultivar Agata) and sufficient for us to observe an electroosmotic flow.
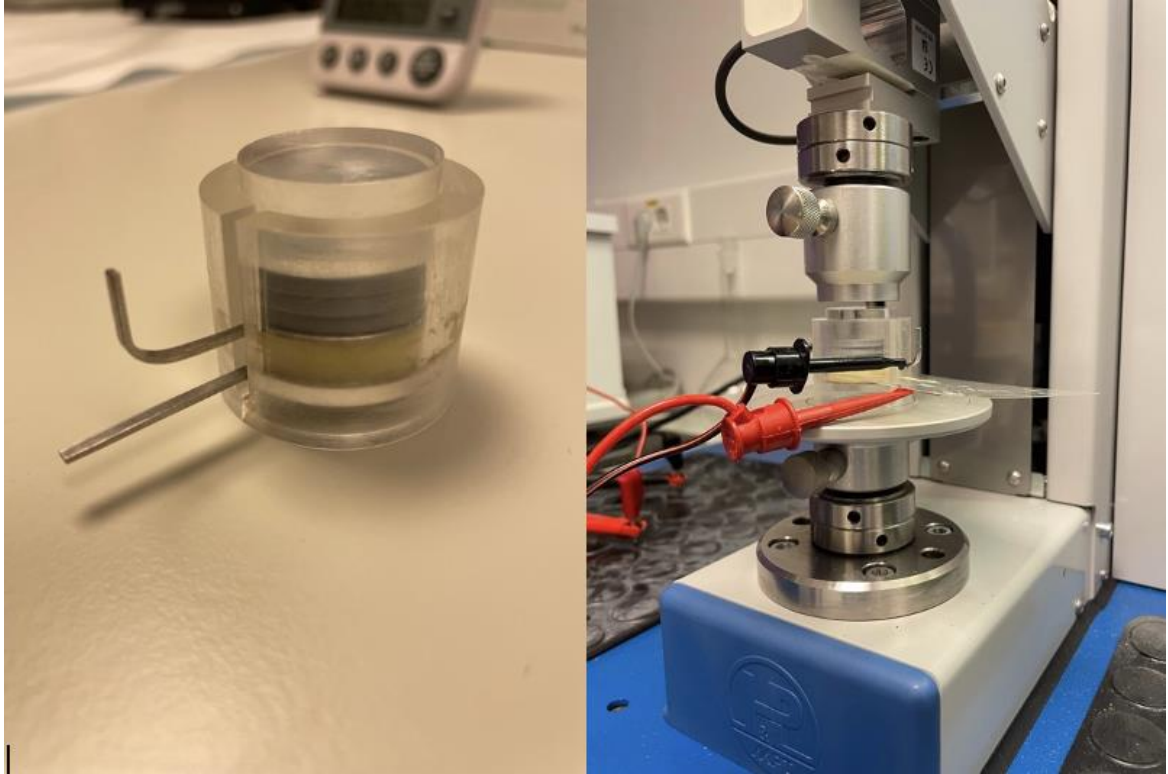
## 2.1.1.    *Treatment chamber*



Figure 4: on the left a picture of the used treatment chamber. On the right the texture analyser with the treatment chamber ready for the experiment. The black connector connects the electrode the negative pole of the generator, while the red one connects the electrode to the positive pole of the generator. The polarity as shown in the figure is thus cathode-top, anode-bottom.

Every protocol required the use of the treatment chamber shown in Figure 4, which was put under the pressure of the piston of the texture analyser (Hegewald & Peschke, model Inspect solo 1 kN-M).

The potato sample was inserted in the plastic chamber between two plate electrodes. Since a flow of liquid was expected, one of the two electrodes was pierced in such a way as to facilitate the passage of liquid from the sample and out of the treatment chamber. Since the electrode was pierced (with holes in its surface), the effect of the electric field on the sample would not have been completely homogeneous, so a very thin metal fabric of a very tight weave (small open void surface fraction) was placed between the sample and the pierced bottom electrode to achieve field homogeneity. If the specimen is only inserted between the two electrodes and the lid is put on, the thickness reached in the cavity of the treatment

chamber is not sufficient that the piston could directly exert a force on the specimen, since the piston is of a larger diameter than the tissue sample. To solve this problem, three plastic discs (grey disks in figure 3) and an additional disc made of acrylic glass were added so that the top where the piston met the chamber was always slightly above the chamber's upper lip (see figure 3-right).

The polarity was set up according to the planned set of the experiments (either the bottom or the top electrode was positive and vice-versa). Two different configurations were used during the experiments: the electrode configuration shown in Figure 4, on right hand side, was called configuration A. In this configuration, the positive pole (anode) is on the bottom electrode, while the negative pole (cathode) is connected to the upper electrode. In the second configuration, configuration B, the anode is the upper electrode, and the cathode is the lower electrode.
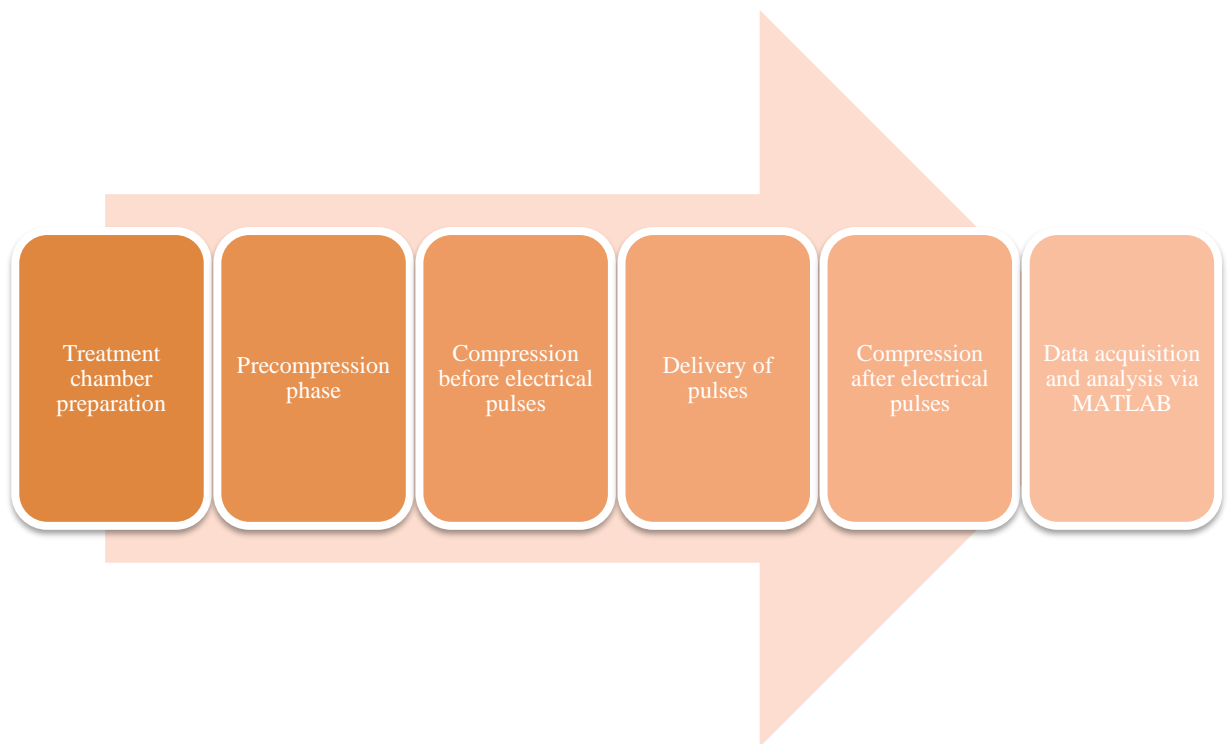
## 2.2. First protocol



Figure 5: Flow chart of the first protocol

The objective was to electroporate cells in the tissue and detect the presence of a flow using a texture analyser (Hegewald & Peschke Inspect solo 1 kN-M) during the individual pulses. This machine can impose a force using a piston and record data on piston displacement continuously during sample compression in the treatment chamber, as well as record the load on the sample applied via the piston (for subsequent analysis or just control whether the force was kept constant). The force of the piston could reach at maximum 1kN (100 kg), but due to biological tissue being quite soft, and expected pressure of electroosmosis being much much lower than that of the texture analyser, much lower forces were used in the range from 5 N (.5 kg) and under 30 N (3 kg).

By supposing the reference system of axes shown in figure 6, the piston imposed a force in the negative z-direction. When electroosmotic flow occurred as a result of the delivery of high-voltage pulses, there was a force along the z-axis that might or might coincide with or oppose to the compressive force caused by the piston, depending on the direction of the applied electric field. In this protocol, every experiment had a duration of 2 minutes.
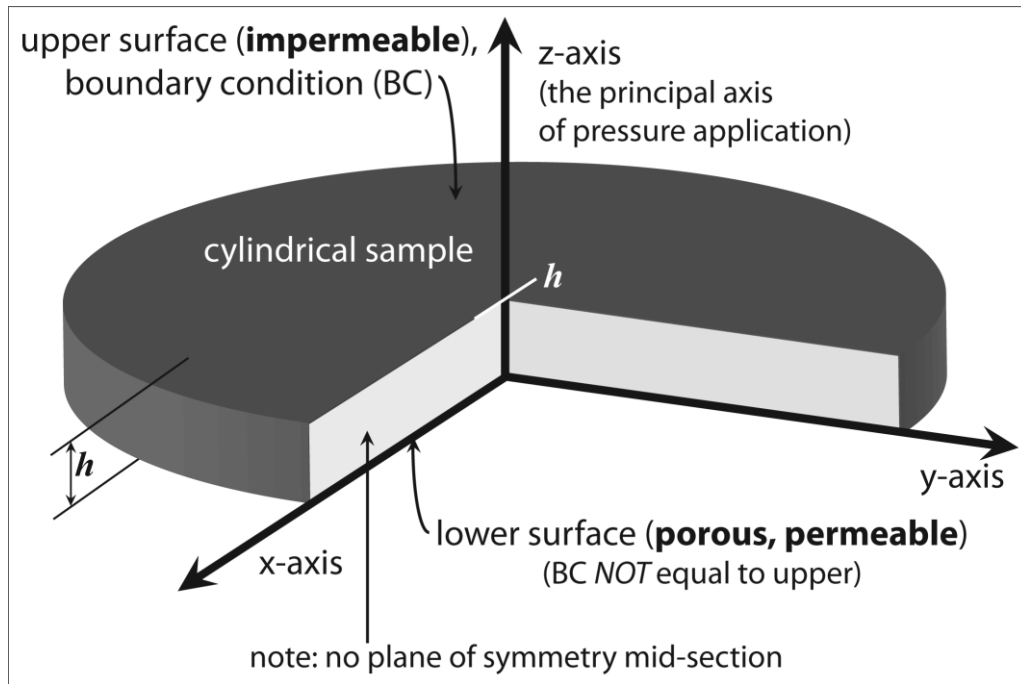
Figure 6: Geometry of the sample with a reference system of axes. Figure reproduced from [Mahnič-Kalamiza et al. 2015] with the author's permission.

The treatment chamber preparation step consists in the setup of the treatment chamber as described in the subsection 2.1.1.
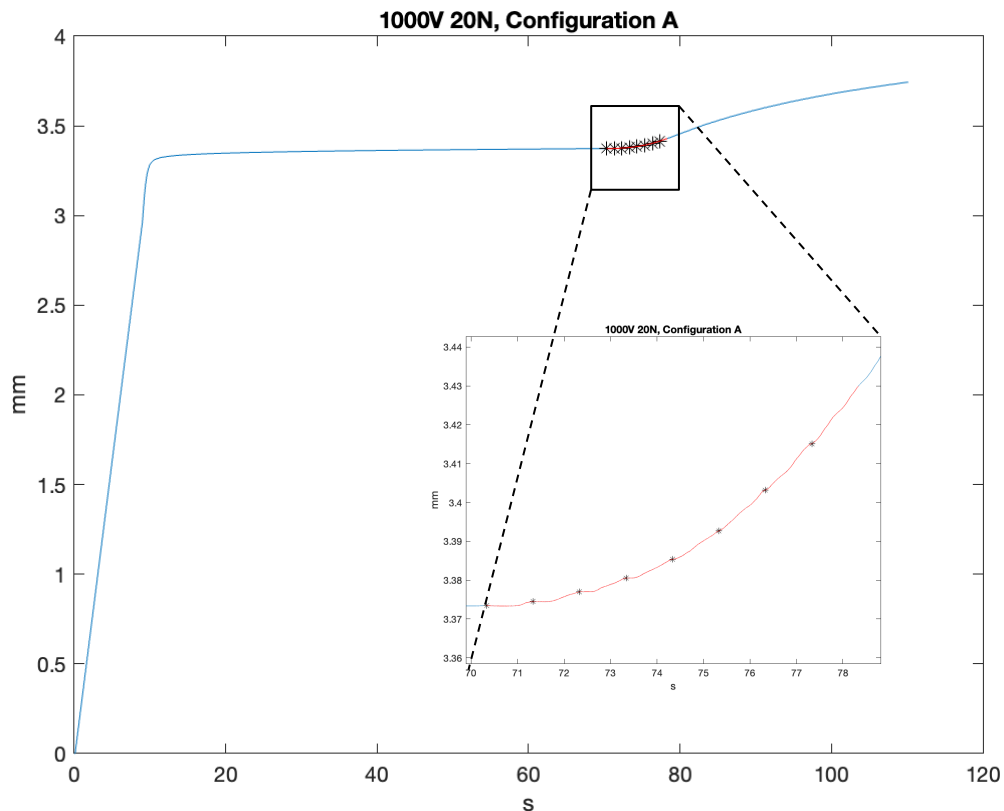
Figure 7 example of protocol 1 recorded data: time is on the abscissa and displacement on the ordinate axis. The displacement corresponds to the movement of the piston and after making contact with the sample, to the compression of the treated plant tissue sample. The precompression phase is later discarded during analysis, then from the remainder of the graph it is possible to distinguish 3 different phases: compression before the delivery of the pulses, where after an initial compression, a plateau is reached; then the delivery of the pulses, which is the "asterisks zone", where every asterisk corresponds to a single pulse; and the last part, which is the final compression after electroporation

## 2.2.1.    Pre-compression phase

The pre-compression phase is the phase where the piston is approaching the treatment chamber with a slow movement, at a velocity of 2 cm/min. The texture analyser is set in a way to start recording when a load of 2 N is reached, which is set to be the point at which the piston comes into contact with the top of the stack of plastic spacers that ultimately transfer force downward onto the sample.

## 2.2.2.    Compression before the electrical pulses

During this phase the texture analyser compresses the treatment chamber (or, rather, the plastic spacers sitting atop the tissue sample) until reaching the previously set force (10 N or 20 N, depending on the set of experiments).

27

Referring to the graph showing the compression of the sample (Figure 7), typically in this phase it is possible to identify a sloping straight line during the first few seconds of the experiment where the cells of the sample are packed, decreasing the space between cells, until reaching a plateau, which is typically then held for 60 s before applying a train of electroporation pulses.

## 2.2.3. Delivery of electrical pulses

A train of electrical pulses is then delivered after the plateau phase of the pre-compression using a high-voltage generator (prototype device), developed in the Laboratory of Biocybernetics of the University of Ljubljana, Faculty of Electrical Engineering. The generator is set to deliver a train of 8 pulses at a repetition rate of 1 $s^{-1}$. The voltage can be changed according to the experiment: typical values chosen for the purposes of this work were 500 V, 750 V, and 1000 V. The figure 7 is showing a test where a voltage of 1 kV was used, and every individual pulse is denoted with an asterisk.

The voltage and the current are recorded during the experiment using an oscilloscope (Teledyne LeCroy HDO6104A-MS), and the temperature using a thermometer (OpSens), whose probes (2) were placed between each of the electrodes and the tissue sample. These measurements were done not only for subsequent analysis, but also for control so as to ensure that proper delivery of pulses always took place and that there was no significant heating of the tissue sample.

## 2.2.4. Compression after the electrical pulses

The piston is continuing the pressure application untill the end of the experiment, maintaining the same load set at the beginning of the experiment.

The previous, electroporation stage, caused a permeabilisation of the cell membrane. The internal structure of the sample is thus less rigid, and a marked and rapid increase in sample compression is expected, as shown in the final part of the compression curve presented in Figure 7.

## 2.2.5. *Data acquisition and data analysis via MATLAB*

During every experiment different data are acquired: load and compression data via texture analyser, electrical data (voltage and current) via oscilloscope, and temperature data via the thermometer.

Both texture analyser and thermometer are connected to a computer and data are recorded by specific software: LabMaster 2.9.2.3 is the texture analyser software, and OpSens' SoftProSens is the software that comes bundled with the thermometer. These environments can provide a human-readable export in .txt files, which can be imported into the MATLAB environment.

The oscilloscope Teledyne LeCroy HDO6104A-MS also supports recording electrical data in a format that can be saved in a .dat format, compatible with the MATLAB environment. Once all the data is imported into MATLAB, the first issue is to find a solution to the synchronisation of the signals since the sources were not synchronised automatically.

By knowing the approximate start and the end of the delivery of the pulses, it's possible to distinguish the three main steps, and consequently develop semi-automated code to synchronise data, so the aim is to find and track the pulses in the compression graph of every test.

Every test was checked manually to find the first impulse and knowing that all the pulses are 1 second apart (with high precision), with a simple few lines of code it was possible to define the moment of the start and end of pulse application (Figure 8).
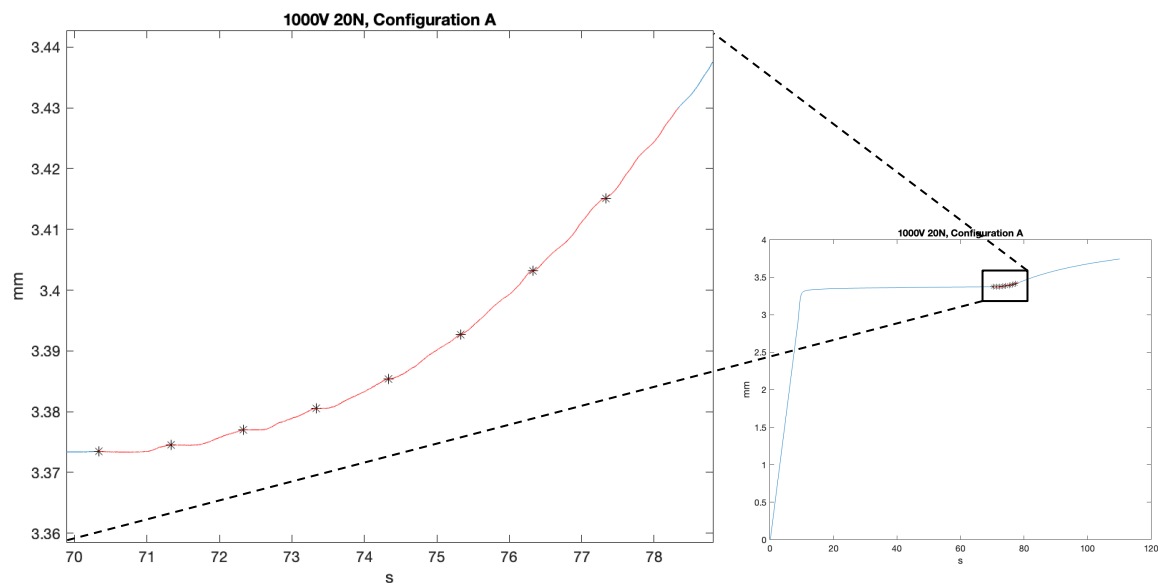
Figure 8 Zoomed-in view of the Figure 7. The first blue part represents the plateau stage before the delivery of the pulses. Once the train of pulses is delivered, the graph shows an increase of the compression in the plant tissue.

Once synchronization was achieved, several curves were analysed, derived from the data obtained during the experiments:

1. Ratio between current and voltage for each sample, to check for linearity and consistency in electrical impedance of the treated samples.

2. Ratio between positive compression and current, where positive compression means the difference between the compression value reached at the end of the pulse and the compression value at the beginning of the pulse.

3. Relationship between positive compression and power, to see whether electroosmotic contribution to compressive pressure is correlated to the electrical power of the delivered pulse.

4. Ratio between negative compression and current, where negative compression means the displacement of the texture analyser piston counter to the direction of the force application. Negative compression is calculated as the sum of all negative movements in piston displacement during a single pulse, calculated as the sum of all differences between neighbouring points on the compression curve whose derivative with respect to time during a single pulse is negative.

5. Relationship between negative compression and power.

6. Relationship between temperature and power, evaluated for both temperature sensors.

7. Mean and standard deviation of temperature.

30

The following table shows the parameters set during the different sets of experiments performed:

| FIRST PROTOCOL | | | |
|---|---|---|---|
| **Set** | **HV Generator** | **Force** | **Polarity configuration** |
| **1** | 1000V | 20N | A |
| **2** | 1000V | 20N | B |
| **3** | 1000V | 10N | A |
| **4** | 1000V | 10N | B |
| **5** | 700V | 10N | A |
| **6** | 700V | 20N | A |
| **7** | 500V | 10N | A |
| **8** | 500V | 20N | A |
| **9** | 1000V | 10N | A |
| **10** | 1000V | 10N | B |
| **11** | 1000V | 20N | A |
| **12** | 1000V | 20N | B |
| **13** | 500V | 10N | A |
| **14** | 500V | 10N | B |
| **15** | 500V | 20N | A |
| **16** | 500V | 20N | B |

Table 1 table showing the parameters set during the various experiments. See Figure 12 in Results chapter for a visual explanation of the polarity configuration.
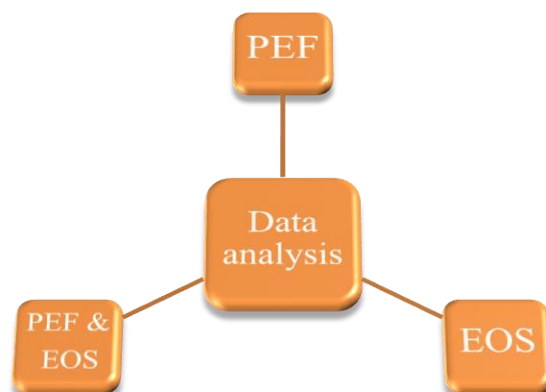
## 2.3. Second protocol



Figure 9: A schematic view of the second protocol. Three clusters are evaluated. A set of experiment requires only the electroporation (PEF), a set requires only electroosmosis (EOS) and the last one requires both the processes in sequence (first electroporation and subsequently the electroosmosis)

In this protocol three different configurations of experiment are evaluated.

The first set of experiment involves the use of the high voltage generator in order to reach electroporation of the sample, just as in the previous protocol, the second one involves the use of the low voltage generator so as to generate electroosmotic flow within the sample without first electroporating the sample, and the last set involves the use of both generators; after a compression phase the high voltage generator is activated to electroporate the cell membranes, and subsequently the low voltage generator is activated to induce the flow through the sample. These two generators are both connected to the sample via a switch box, which, by means of a toggle switch, allows to switch between generators and change polarity without reconnecting any wires to the electrodes.

The last set of experiments requires only the low voltage generator in order to induce the flow without the electroporation step.

In this protocol, every experiment has a duration of 6 minutes.

According to the analysed configuration, the parameters which can change are:

- Force imposed on the sample by the texture analyser: 10 N or 20 N

- Voltage on the HV generator: 600V or 900V

- Voltage on the LV generator: 10V or 15V

- Polarity: configuration A or configuration B

Each configuration is based on the one described in the subchapter 2.2.

Small adjustments are necessary depending on the process involved in the experiment.

The preparation of the treatment chambre (2.1.2) and the precompression phase (2.2.1) are included in every experiment and these steps precede the compression phase of the texture analyser.

## 2.3.1. Electroporation configuration (PEF)



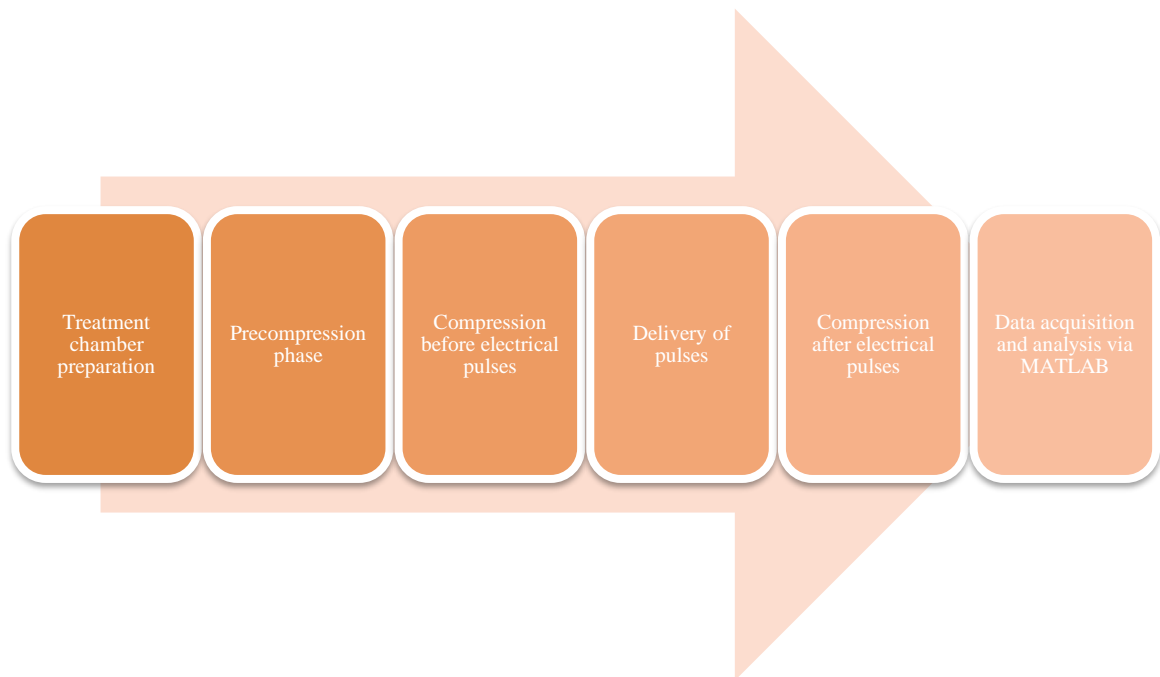| Treatment chamber preparation | Precompression phase | Compression before electrical pulses | Delivery of pulses | Compression after electrical pulses | Data acquisition and analysis via MATLAB |

Figure 10: Flow chart of electroporation configuration

The texture analyser is set up according to the experimental plan and activated. After the precompression phase, the compression phase has a duration of 30 seconds, thereafter a train of 8 pulses with a repetition rate of $1 \text{ s}^{-1}$ is delivered.

The texture analyser keeps maintaining the compressive force until reaching minute 6, at which point the experiment is terminated.

The aim of this experimental set is to record some typical electroporated sample curves for analysis of electroosmotic effects during pulse application.

## 2.3.2. *Electroporation and electroosmosis configuration (PEF & EOS)*
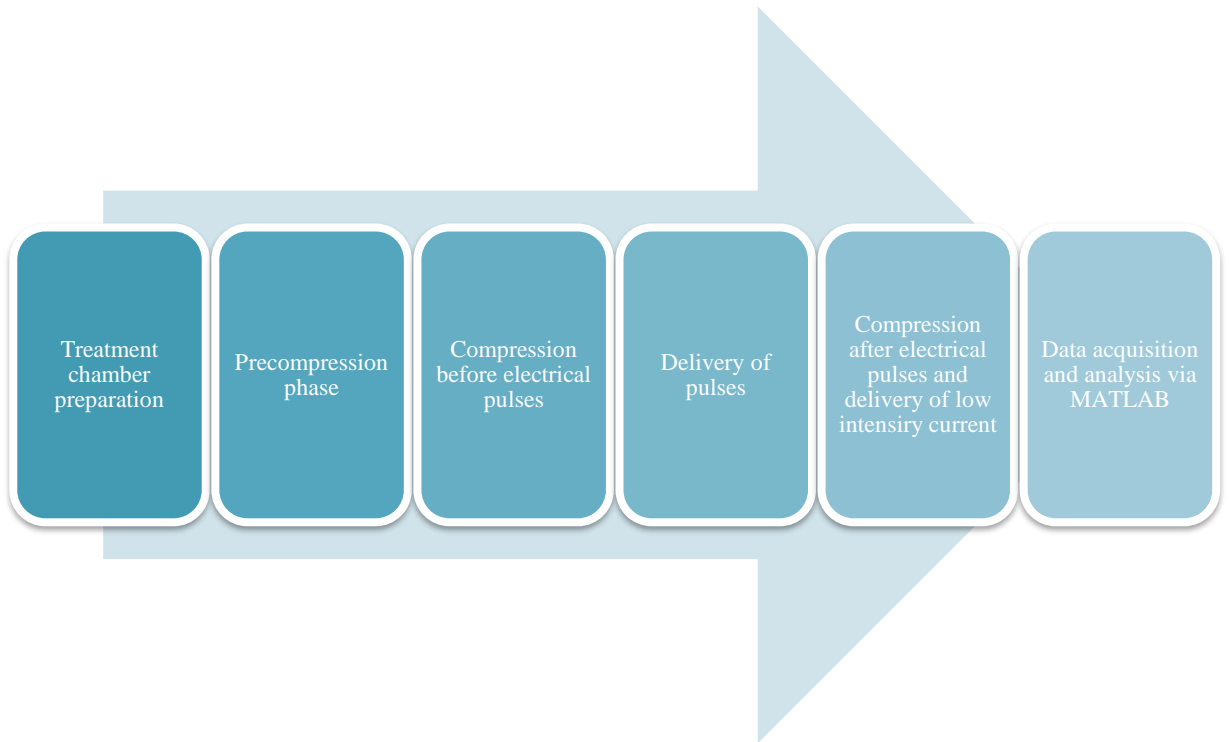


Figure 11: Flow chart of electroporation and electroosmosis configuration (PEF & EOS)

After an initial configuration the texture analyser is activated. Once the precompression phase has passed, the treatment chamber is loaded by the piston for 30 seconds. Past this time, a train of 8 pulses with 1 s$^{-1}$ repetition rate is delivered with the HV generator in order to electroporate the cell membranes in the tissue.

Immediately after the train of pulses, via the switch box, the LV generator is activated to stimulate the process of electroosmosis, meanwhile, the piston of the texture analyser is still exerting pressure on the sample until reaching 6 minutes (end of experiment).

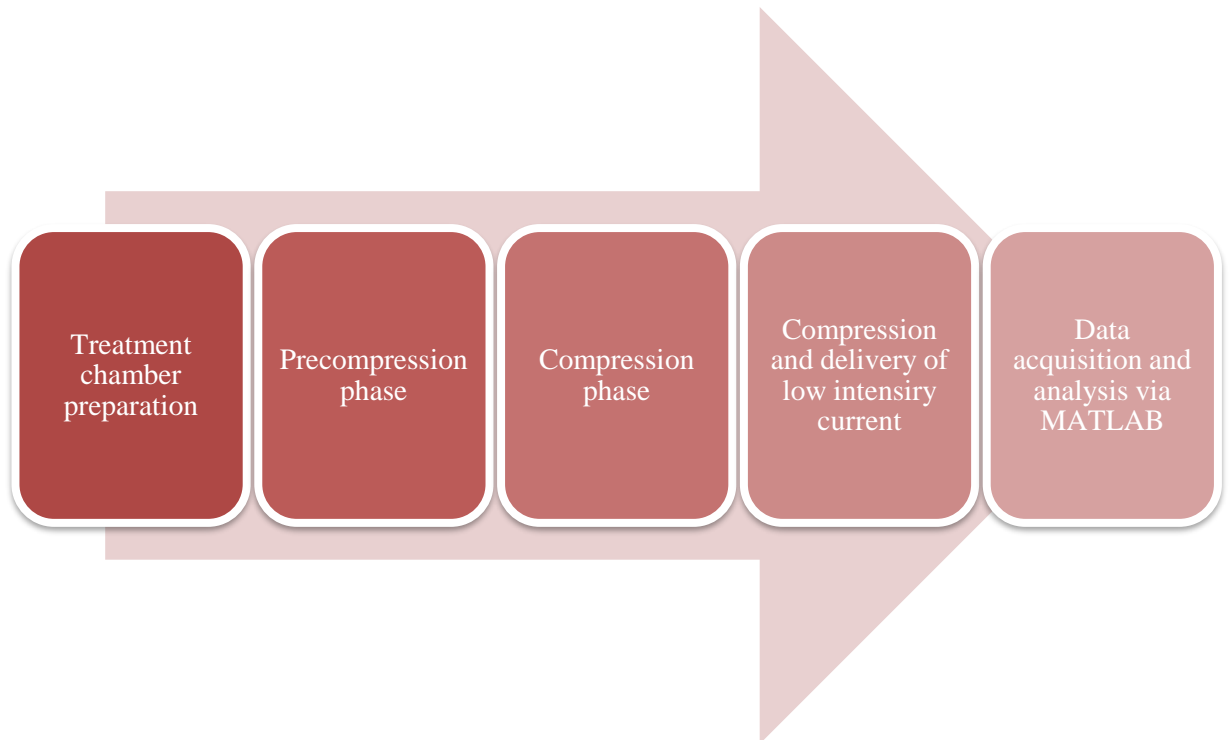### 2.3.3. *Electroosmosis configuration (EOS)*



Figure 12, Flow chart of electroosmosis configuration (EOS)

With this set of experiments an electroosmotic flow is supposed to be induced without applying the electroporation process.

Once the texture analyser is activated and the precompression phase is passed, the treatment chambre is pressed for a period of time of 38 seconds, which is equivalent to the sum of the duration of the compression phase before the release of the impulses and the duration of the delivery phase of the electrical impulses.

After 38 seconds, the low-voltage generator is activated, so that electroosmotic flow is induced while the piston is still exerting pressure. This phase ends at the reaching of 6 minutes.

## 2.4. Data acquisition and data analysis via MATLAB

As with the previous set of experiments, during every experiment miscellaneous data are acquired: load and compression data via texture analyser, electrical data (voltage and current) via oscilloscope, and temperature data via the thermometer.

Data are recorded and exported/imported into the MATLAB environment, and the synchronization is derived manually, as already described in the subchapter 2.2.5.

Once synchronization was achieved, several curves were analysed, derived from the ratios of the data obtained from the experiments:

1. Differences in terms of compression between only-PEF and PEF & EOS configurations, in the time domain from the end of the pulses to the end of the pulses plus 30 seconds.

2. Differences in terms of compression in PEF & EOS configuration, in the time domain from the end of the pulses to the end of the pulses plus 30 seconds, highlighting the effects of different configuration of polarity.

3. Differences in terms of compression in PEF & EOS configuration, in the time domain from the end of the pulses to the end of the pulses plus 180 seconds, again highlighting the effects of different configuration of polarity.

4. Mean and standard deviation of the compression in only-PEF, only-EOS, PEF & EOS configurations considering the range from the end of the pulses to the end of the pulses plus 30 seconds.

5. Mean and standard deviation of the compression in only-PEF, only-EOS, PEF & EOS configurations considering the range from the end of the pulses to the end of the pulses plus 180 seconds.

6. Area analysis of the compression in PEF & EOS configuration after the electroporation in the range from the end of the pulses to the end of the pulses plus 150 seconds.

7. Mean and standard deviation of the "incremental compression 1" in only-PEF and PEF & EOS configurations. Calling "end point" (EP) the end of the delivery of pulses, "incremental compression 1" is calculated as the compression difference

between the compression value in EP + 30 s * *i* (where *i* is an integer) and a reference compression value in EP.

8. Mean and standard deviation of the "incremental compression 2" in only-PEF and PEF & EOS. This "incremental compression 2" is calculated as the compression difference between the compression values of two points delayed by 30 seconds.

9. The ratio between the area under the current curve and the compression evaluated in all the configurations.

The following table shows the parameters set during the different sets of experiments performed:

| SECOND PROTOCOL | | | | |
|---|---|---|---|---|
| Set | HV Generator | LV Generator | Force | Polarity configuration |
| 1 | 900V | / | 10N | A |
| 2 | 900V | 10V | 10N | A |
| 3 | 900V | 10V | 10N | B |
| 4 | / | 10V | 10N | A |
| 5 | / | 10V | 10N | B |

Table 2: Table showing the parameters set during the various experiments.

## 2.5. Switch box for switching polarity configuration and generator source

During experimentation, it was necessary to be able to easily switch, without physically changing cable connections of the electrodes to the generators, both between the pulsed power generator and the DC-current generator, and to be able to switch polarity of the top and bottom electrode without reconnecting any cables. For this purpose, the switchbox illustrated by photographs presented in Figure 13 below was assembled. It is a simple circuit with two pairs of input connections (red/black for +/-) for the generator, a pair of output connections for the two electrodes, and two toggle switches. Both switches are of the DPDT (double-pole, double throw) type, one is an ON-NONE-ON configuration (MulticompPro 1MD1T1B1M1QE) and the other an ON-OFF-ON configuration (MulticompPro 1MD3T1B5M1QE). The first (ON-NONE-ON) functions as the polarity selector switch, and the ON-OFF-ON as the generator selector switch, with the middle position (OFF) being used in case voltage/current on the electrodes need to be disconnected from the generator.



Figure 13: The switchbox used for easy changing of polarity and generator source.

# Chapter 3

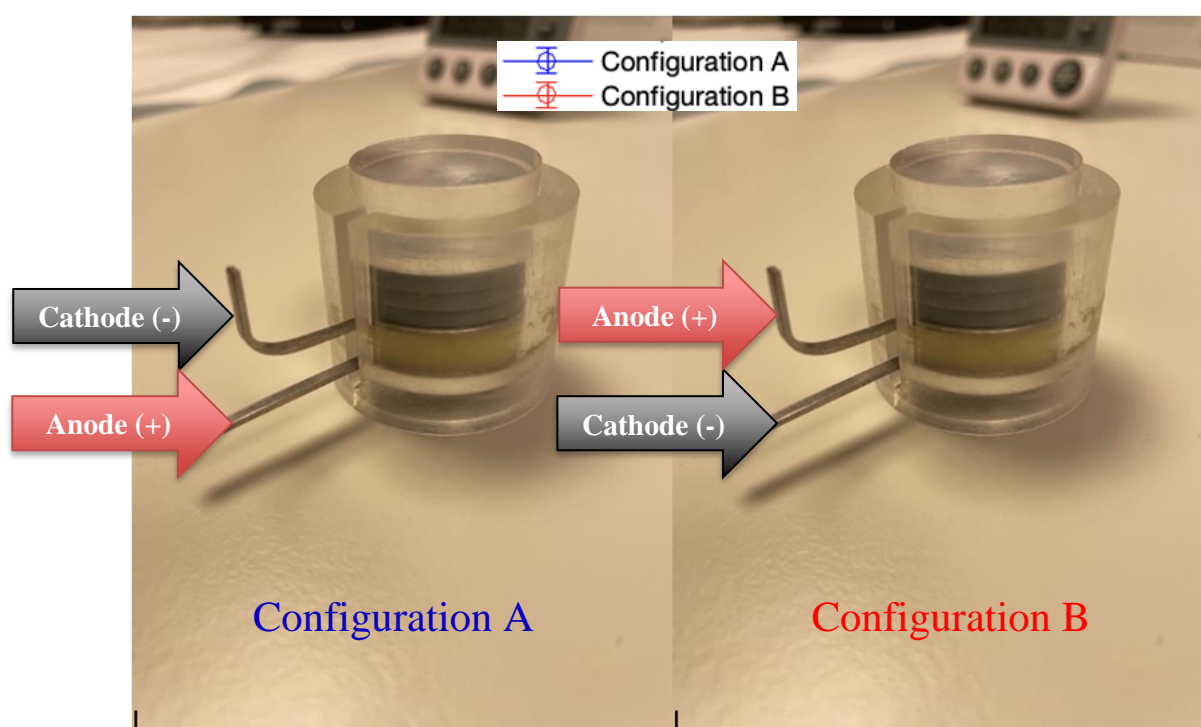# Results and discussion

## 3. Results and discussion



Figure 14: A schematic representation of the two configurations used during the experiments

In this section, the results obtained during the experiments are presented. To make the next graphs easier for the reader to understand, Figure 14 shows the two different polarity configurations used for these experiments.

# 3.1. Demonstration of electroosmotic effect of plant tissue under force exerted by the texture analyser during PEF application
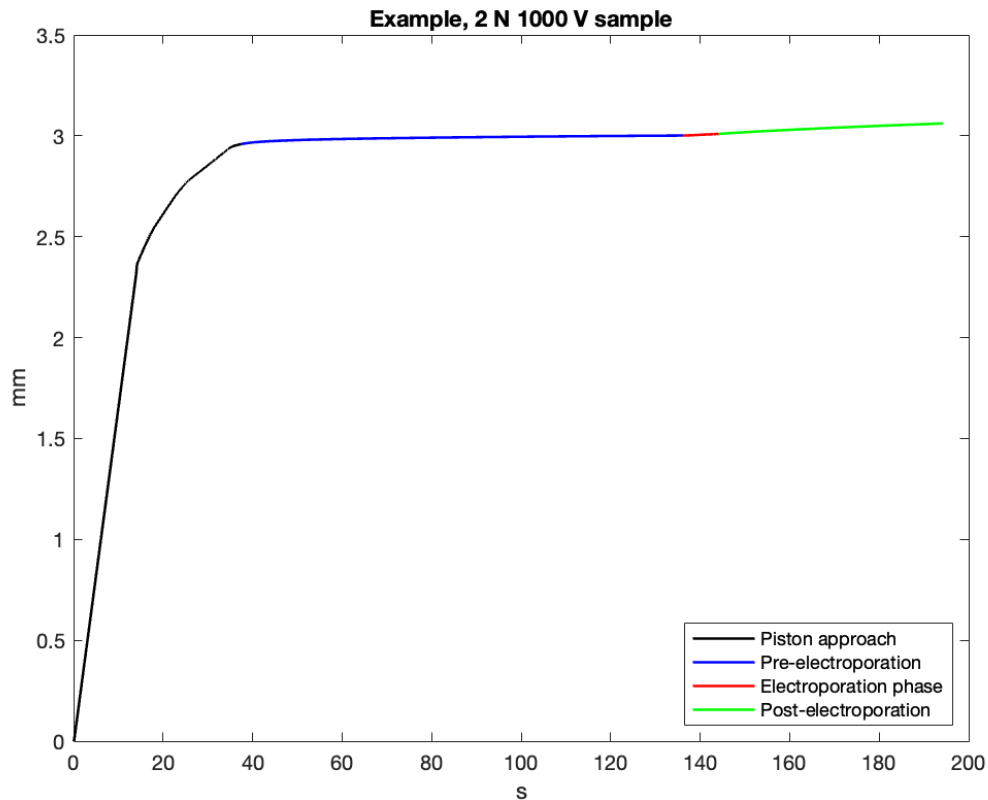


Figure 15, example of a curve obtained using texture analyser

Figure 15 shows the typical behaviour of plant tissue subjected to a compression test with the texture analyser. On the abscissa is time and on the ordinate the displacement in millimetres. The procedures described for the first protocol (subsection 2.2) were performed in this case with the following parameters:

- Compressive force applied by the texture analyser: 2 N
- Voltage delivered by the high voltage generator: 1000 V
- Sequence of 8 pulses with repetition rate of 1 $s^{-1}$

Four distinct stages can be observed in the curve: initially, the sample is exposed to an increasing compressive force as the machine's piston has to reach the pre-determined (set target) value. During this stage, the piston moved by around 3 mm, but did not cause any compression of the sample. Once the pre-set force value is attained, it is kept constant for a minimum of one minute. Plant cells have a pressure referred to as turgor pressure, which is defined as the pressure exerted by the liquid inside the cell on the cell wall. On the contrary, the cell wall exerts a resistance that counterbalances the turgor pressure to prevent lysis of the cell. Therefore, the pressure exerted by the texture analyser piston on the sample increases the turgor pressure, but the resistance of the cell wall ensures that the compression value remains constant. Subsequently, the train of 8 pulses is delivered by means of the high-voltage generator. The electroporation process, when interacting with plant tissue, causes the disruption of the cell membranes, thus permitting the outflow of the intracellular liquid. Turgor pressure is substantially reduced, and some cells undergo an explosive loss of liquid and complete loss of cell homeostasis. During pulse application, an electric field stimulates the movement of the intracellular liquids by means of electroosmosis in the direction of the cathode, which should be manifesting as either a counter-pressure or an additional compressive pressure to that of the piston. After the application of the electric pulses, the pressure is sustained for an additional 40 seconds to allow for the full manifestation of the electroporation-induced cellular membrane breaches, resulting in a discernible increase in compression of the sample.
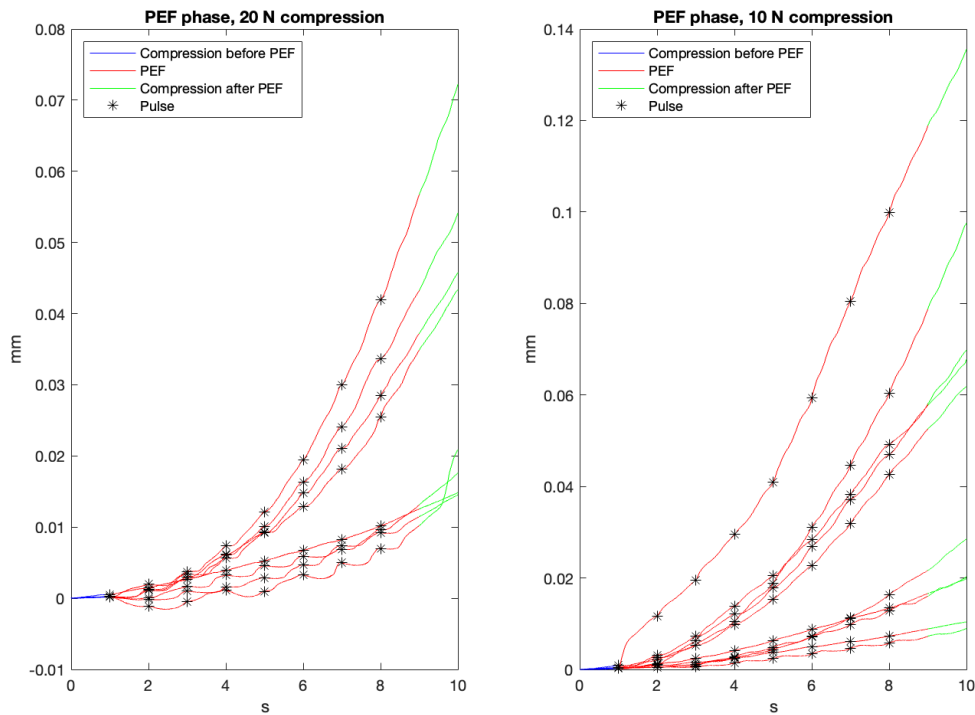
Figure 16, a comparison between samples with 20 N and 10 N. For both forces, the samples were treated with voltages of 1000, 700 and 500 V.

Figure 16 presents a comparison of pulse delivery phases in samples treated with the same set of voltages (1000 V, 700 V, or 500 V), but applying different forces (20 N – left, or 10 N – right). Curves with a steeper slope correlate to higher voltage values. This is in line with what was previously described, wherein higher voltage is associated with higher probability of cellular membrane disruption, leading to a larger drop in turgor pressure, and ultimately, increased compression of the sample. Except for one case, with 10 N compression, where the compression values obtained were significantly higher, the remaining samples were comparable. With 20 N compression, negative compression values were observed for samples treated with low voltage pulses (500 V), a contrast to the samples treated under 10 N of compression; notice the "dips" in the compression curves in figure 14-left. One possible explanation we have to offer for this observation is that, as opposed to the lower compressive force of 10 N, with the higher compressive force of 20 N, the contact between tissue and electrodes is much better. Also, the higher force is maintaining the sample more homogeneous in terms of liquid distribution. This means the electric current is higher during pulse application, since the electrical resistance of such a sample would be lower. This results in a more pronounced effect of electroosmosis, but

since with higher voltages such as 1 kV the effect of turgor pressure loss is so significant, this effect of negative displacement is obscured by it, and is only observable in the case of lower voltage of 500 V, where the majority of the tissue sample has not been electroporated, and turgor tissue not so drastically liberated. In other words, the counter-force of the electroosmotic flow to the pressure of the piston is "hidden" by turgor pressure loss in cases where tissue is more drastically affected by electroporation using higher pulse voltages.

A comparison was then made between the electroporation of animal tissue and the electroporation of plant tissue, and the different reactions to the process were observed. The data on animal tissue were obtained from experiments that had been conducted previously in the Laboratory of Biocybernetics in Ljubljana by Genovese et al. The data were obtained on chicken breast samples that had been subjected to a force of 15 N and a voltage of 800 V, as well as fresh potato samples that had been exposed to a voltage of 700 V and 20 N (experiments performed within the scope of this study). To ensure that the tests were comparable, the current flowing through the animal tissue sample had to be between

60 and 200 % of the current through the plant tissue sample. The current graphs are illustrated in Figure 17.



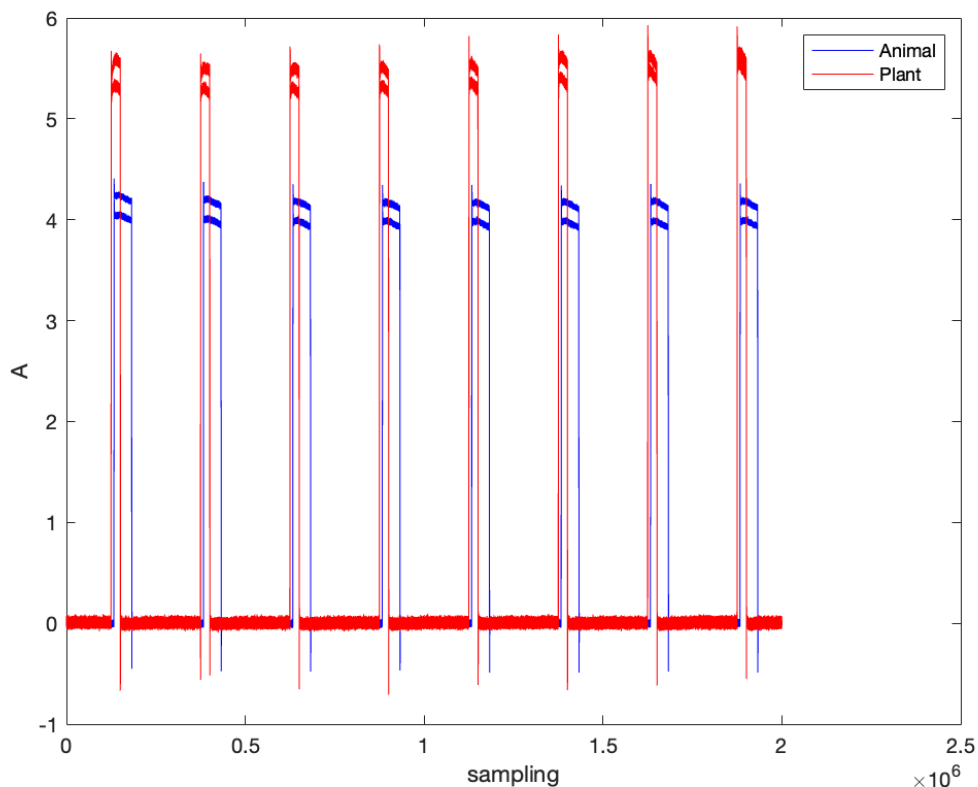Figure 17, Current in the analysed plant and animal tissue

The ratio was calculated by contrasting the lower current value in the animal tissue with the lower current value in the plant tissue and comparing the upper current value in the animal tissue with the corresponding plant tissue current value. The values acquired were 76 % in both cases, thereby confirming the comparability of the data.
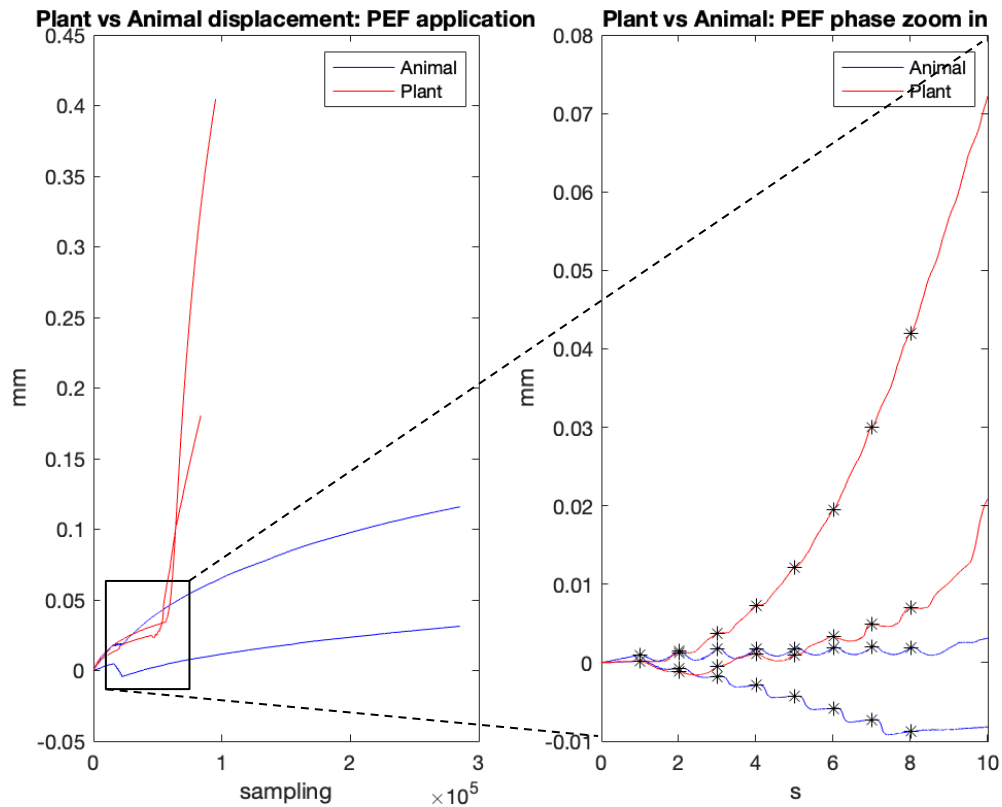
Figure 18, Comparison between animal and plant tissue during the application of the pulses of electroporation. The precompression phase is neglected and the curves normalized. On the left side the graph shows the entire compression while the right side shows the electroporation phase aligned and normalized.

Figure 18 presents a comparison between animal and plant tissue when subjected to compressive force, along with the application of high voltage pulses for electroporation. The graph on the left illustrates the overall behaviour of samples subjected to the test. Plant tissue exhibits a higher compression level as a result of electroporation, due to the drop in tissue turgidity, thus allowing for greater compression. As animal tissue lacks a cell wall, it is not possible to observe the same behaviour as that of plant tissue, and thus the compression value in the absolute sense is lower. The graph on the right displays the various compression curves that have been aligned to observe the behaviour of the tissue at the time of electroporation. Animal cells are not subjected to cell turgor, since there is no resistance, which means that the electroosmotic flow due to the high voltage is more pronounced and has a higher impact on the compression curve. On the contrary, plant tissue exhibits a much more dynamic behaviour due to turgor pressure liberation upon electroporation. This comparison is important, because it demonstrates that electroosmotic

45

flow and resulting superimposed compressive force does occur also in *ex vivo* animal tissues, not only in fresh and turgid plant tissues. A finding that has important consequences for the field of biomedical applications of electroporation.

## 3.2. Characterization of EOS in potato using texture analysis and current/voltage/power analysis

The correlation between compression in millimetres and electrical terms such as current and power was explored in more detail. To assess the relationships, both positive displacement of the piston (positive meaning in direction of expected sample deformation) during pulse delivery, and negative displacement, calculated as the sum of the negative contributions of the compression curve in the duration of electroporation pulse application, were considered. What we expected to see was some correlation, linear or other, between the applied current of the pulses and positive or negative piston displacement during pulse application. Unfortunately, as the following four figures illustrate, none was found.
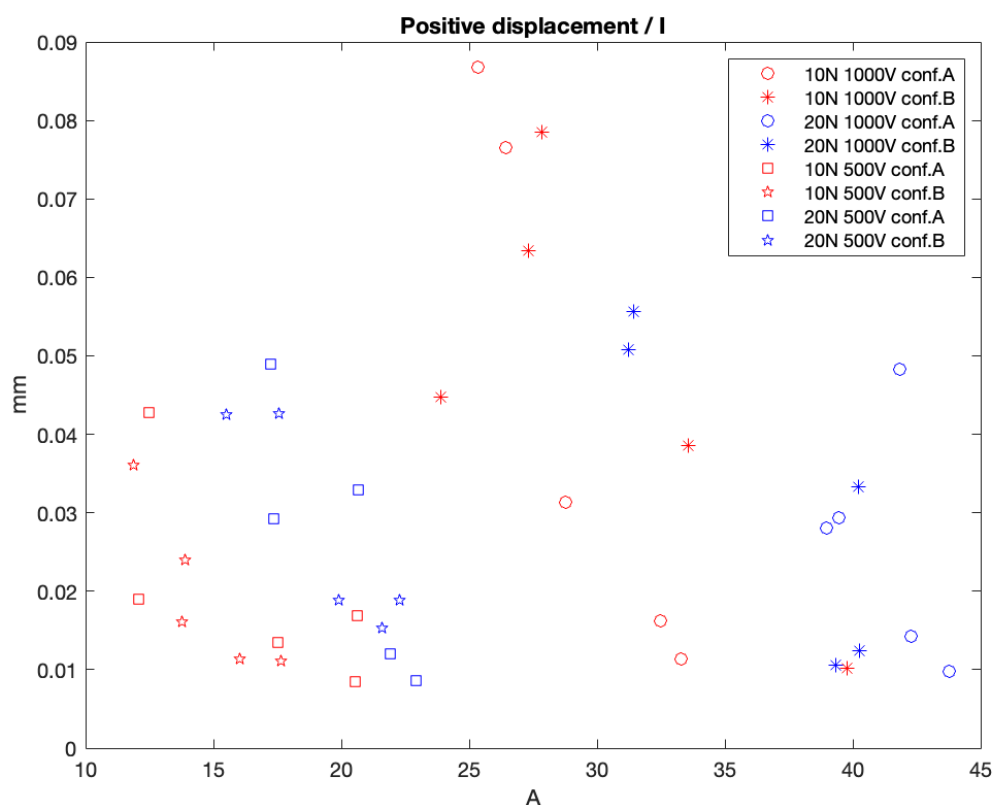


Figure 19: Relationship between positive displacement and current

Figure 19 shows the relationship between the positive displacement and the average pulse current. Experiments were carried out with samples that were subjected to either 10 N or 20 N compression force, and the high-voltage generator set to 500 V or 1000 V, with both polarity configurations (the two anode/cathode–top/bottom combinations). As can be observed, the electric current varies greatly, as these samples are biological in origin and therefore highly variable. From the graph, by a rather generous stretch of the imagination, four distinct clusters could potentially be identified, according to the voltage applied, with polarity not having a major effect since samples with different polarities treated with the same voltage are distributed homogenously within the clusters. The positive displacement does not appear to be dependent on current within the clusters, so data appears to be inconclusive.
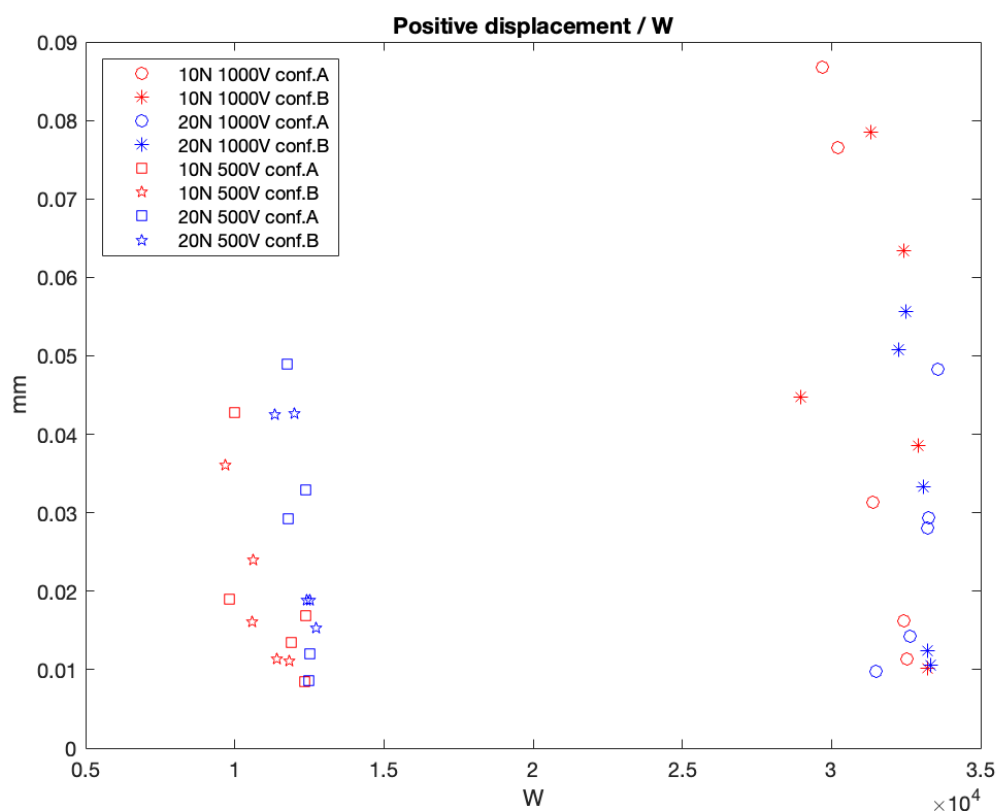


Figure 20:  Relationship of positive displacement and electric power

Figure 20 reveals a clear distinction between two clusters in the relationship between positive displacement and electrical power. This was expected, since the generator was set to 1000 V in one case and 500 V in the other, and due to its relatively high internal output

resistance, the voltage drop on the target tissue linearly scaled in relation to the current through the sample, resulting in two distinct power settings, one at about 1,25 kW, and the other at about 3,25 kW. Polarity does not appear to be a factor in determining the positive displacement values, as was already observed in the analysis of the relationship between positive displacement and current.
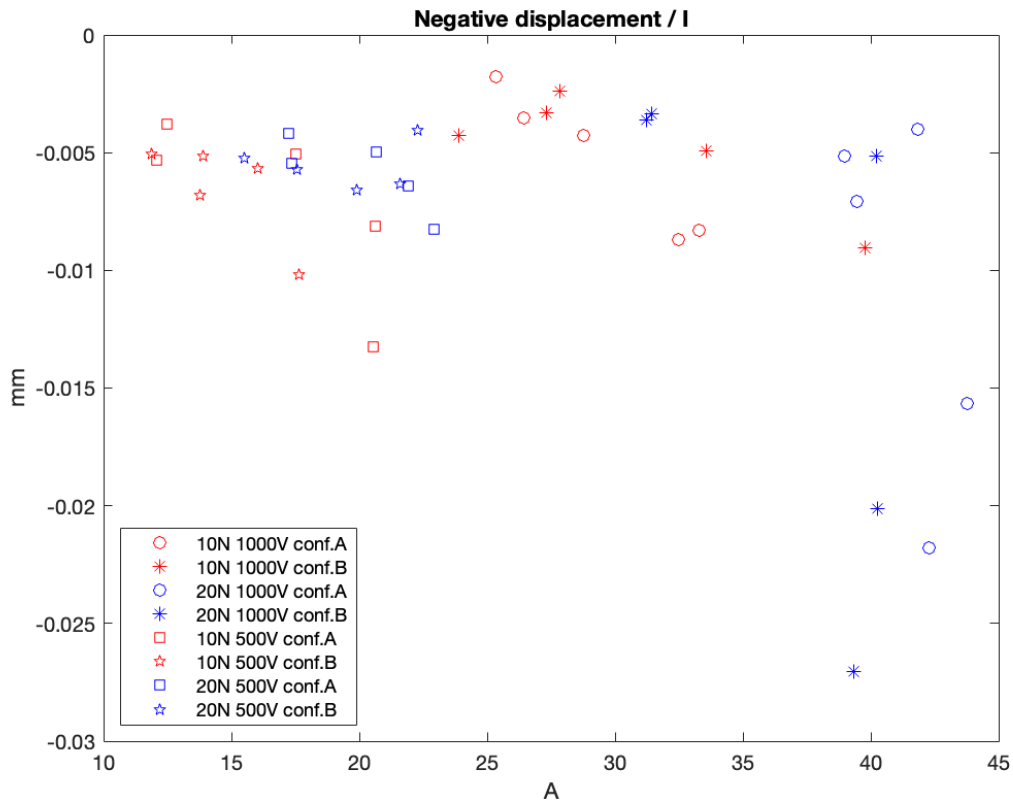


Figure 21: Ratio of negative displacement and current

Similarly to the previous two, Figure 21 depicts the ratio of negative displacement to current and here the clusters become even less distinct. It can be observed, again, that polarity does not appear to have an effect on displacement. The lowest values were achieved when a compressive force of 20 N and voltage of 1000 V were applied, meaning that this most severe combination of pulse amplitude and force application resulted in the most significant "dip" in the compression curve of all, something that was to be expected. Other than the non-significance of the relationship, nothing else can be deducted from this raw data that is not aggregated in any way, but is given for all individual tissue samples individually.
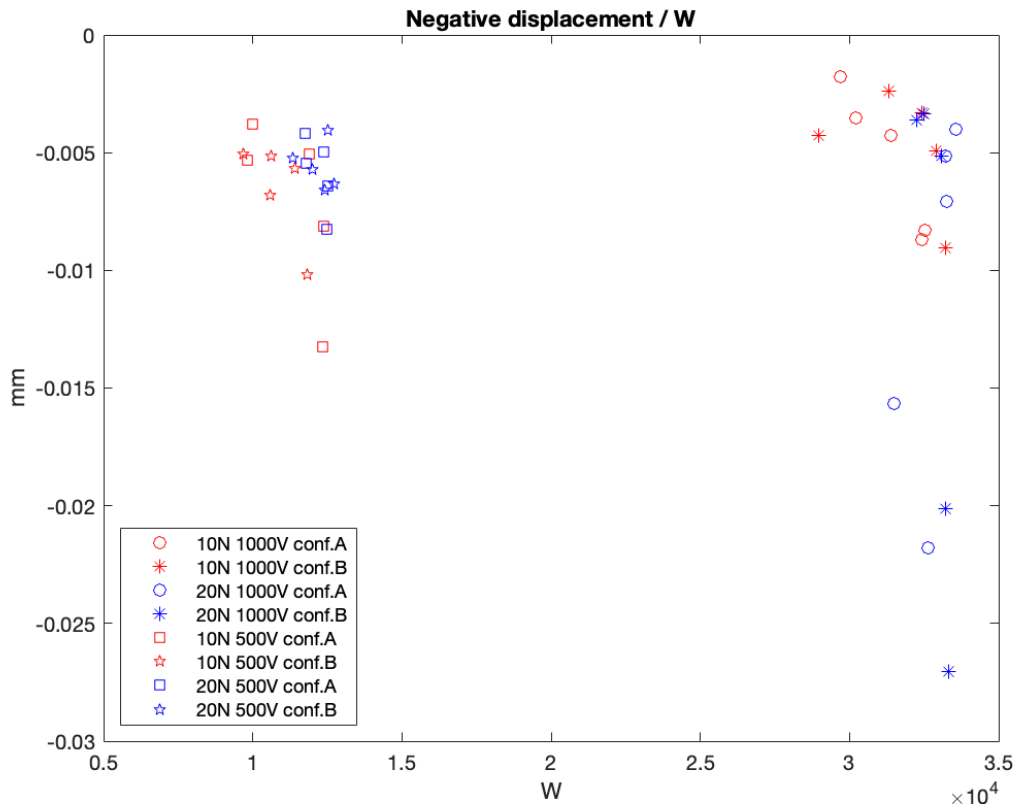
Figure 22, Ratio of negative displacement and electric power

For completeness sake, we also present Figure 22, giving the relationship between negative displacement and electrical power, which also features two distinct clusters as in the relationship between positive displacement and electrical power, which is determined by the application of a specific voltage.

In order to be able to extract any useful information from the gathered data, we must turn to aggregation by common experimental parameters, and analysis of statistically significant differences between the averages.

Figure 23: comparison of the ratio of positive displacement to electrical power, assessed by first averaging samples subjected to the same compression force and then samples with different polarities.

We thus performed a comparison of the ratio of positive displacement to electrical power, by grouping in one case samples that were subjected to the same compressive force, and in the second case samples treated with use of the same polarity configuration. Figure 23 on the left side shows the mean and standard deviation of the results obtained through the aforementioned averaging. The comparison between the samples treated with 20 N and 10 N compression forces indicates that, on average, higher electrical power values were obtained in the samples treated with 20 N, which seems to make sense due to the previously mentioned phenomenon of maintaining better electrical homogeneity and electrode contact with tissue using higher compression forces. However, displacement levels of the 20 N samples were lower than those for the 10 N samples.

The comparison of the averages of samples treated with different polarities (Figure 23, right side) demonstrated that the configuration B resulted in higher compression values, this is because, since in this configuration the cathode is connected to the lower electrode,

51

the electroosmotic flow moves in the same direction as the piston, causing greater compression. Unfortunately, as shown by analysis of statistical significance presented in Table 3, none of these observed differences are statistically significant, and thus no definitive conclusions as to the effect of compressive pressure or electrode polarity can be made. What is still clearly demonstrated by all of these examples from their compression curves though is, that significant disturbances in compression kinetics are brought about by pulse application, thus clearly demonstrating the presence and effect of electroosmotic flow.

Similarly to the analysis presented in Figure 23, the comparison was made between the averages of negative displacement and electrical power (Figure 24).
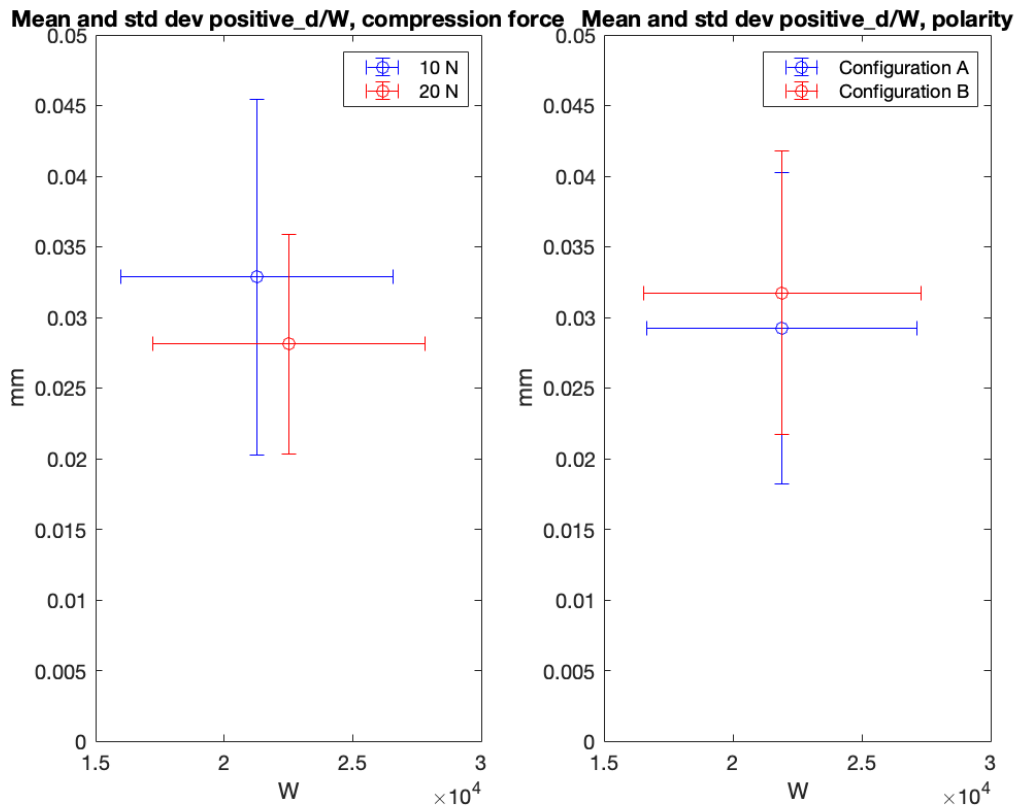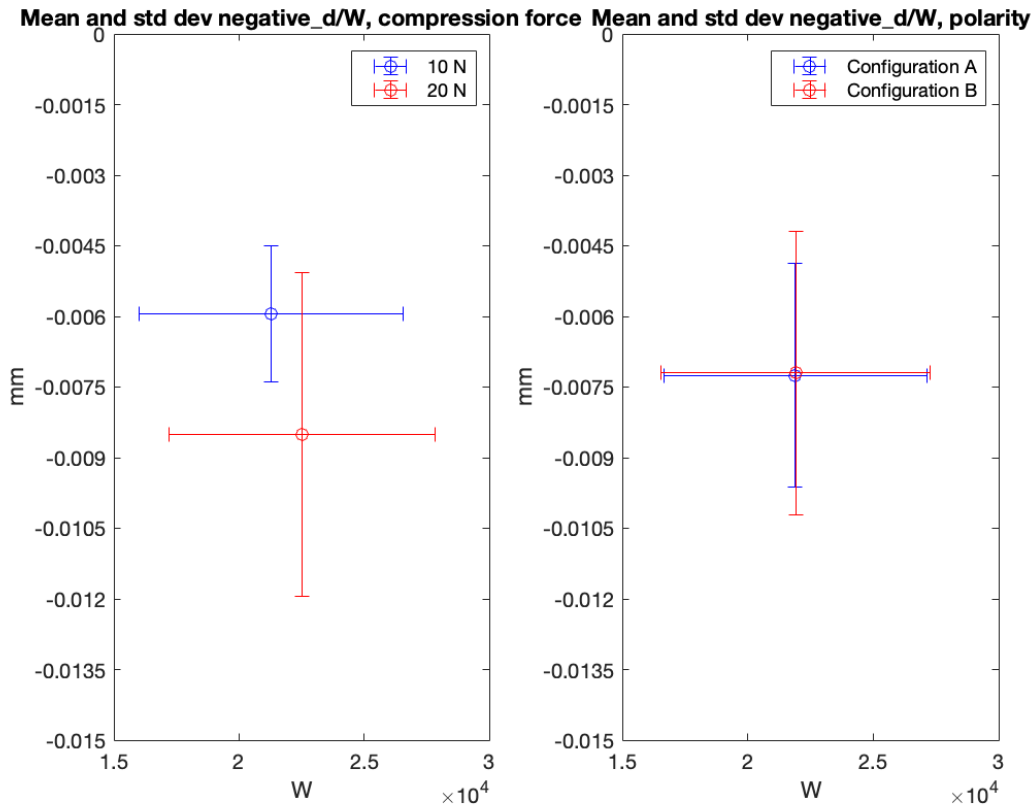


Figure 24: comparison of the ratio of negative displacement to electrical power, assessed by first averaging samples subjected to the same compression force and then samples with different polarities.

In the comparison between samples exposed to different forces, the graph reveals that, on average, samples subjected to 20 N have lower negative displacement values than those

exposed to 10 N. This result is in congruence with Figure 23, as samples exposed to the force of 20 N, at the time of the release of the pulse, are exposed to a force, due to the electroosmotic flow, opposite to the force of the piston, leading to a more significant negative contribution than the corresponding samples subjected to a compressive force of 10 N, implying a more reduced positive displacement in the samples treated with 20 N force. Again, the polarity doesn't seem to be a significant factor in the negative displacement.

As previously mentioned, to determine if observations based on Figures 23 and 24 had any solid, statistically demonstrable merit, it was necessary to analyse the statistically significant differences between the compared groups of averaged data. A statistically significant difference indicates whether the responses of the two groups analysed are sufficiently different from each other through a statistical analysis. To do this, a t-test was performed for each pair of groups of tissue samples analysed, and the results are shown in Table 3.

| STATISTICAL ANALYSIS | | | | | |
|---|---|---|---|---|---|
| Variable 1 | Samples V1 | Variable 2 | Samples V2 | p-value | p-value < α |
| 10 N positive displacement | 20 | 20 N positive displacement | 20 | 0,478790822 | no |
| 10 N negative displacement | 20 | 20 N negative displacement | 20 | 0,131555758 | no |
| Conf. A positive displacement | 20 | Conf. B positive displacement | 20 | 0,70683241 | no |
| Conf. A negative displacement | 20 | Conf. B negative displacement | 20 | 0,975602489 | no |

Table 3: the samples analysed and the number of samples subjected to the t-test are reported for each line.

Statistical significance is calculated with a standard confidence level of 95 %. Accordingly, a difference is assessed as statistically significant if the difference between the two groups has a probability of less than 5 %, which is indicated by a p value of less than 0.05.

Table 3 shows that the p-values are above the threshold of 0.05, which means that the differences are not statistically significant. In particular, in the cases where a statistically significant difference is observed between the group treated with configuration A and the group treated with configuration B, the p-value shows values very close to 1 (0.7068 for the positive displacement and 0.9756 for the negative displacement). Very high p-values can also be seen from the corresponding graphs in Figure 23 and Figure 24, as the means and standard deviations show similar values and the standard deviations overlap at least to some degree without exception.

# 3.3. Electroporation and electroosmosis application with DC generator

Following the second protocol (subsection 2.3), experiments were performed to observe the effects of electroporation followed by electroosmosis. These experiments were performed in addition to the preliminary analysis presented in the preceding subsection because we wished to conclusively show whether the polarity of the electrodes has the expected effect on the compression kinetics by means of altering the direction of the superimposed electroosmotic pressure, cause by the induced electroosmotic flow in tissue.
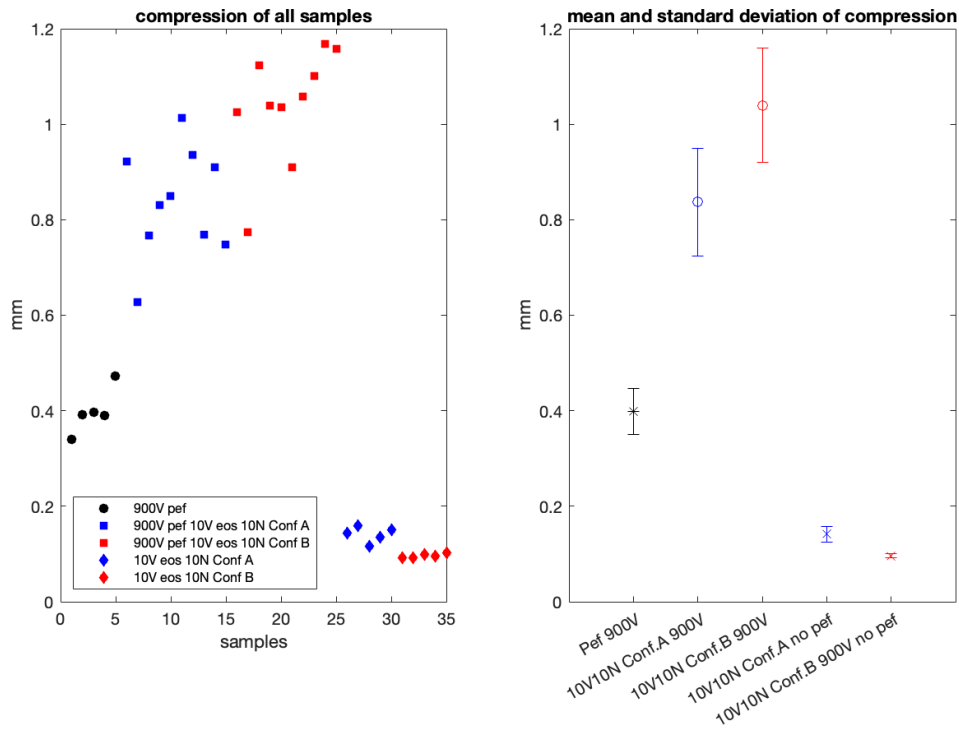


Figure 25: On the left, the compression values of each analysed sample are shown. On the right, the graph shows the mean and standard deviation of the various sample clusters analysed.

Figure 25 shows the compression values obtained in the different cases studied (Table 2), presenting values for both the individual samples, as well as the mean values and standard deviations for the groups of samples studied.

For samples treated with electroporation only, the compression was calculated as the difference between the piston position at the end of the experiment and the piston position at the beginning of the pulse application. For the samples treated with electroosmosis only,

compression was calculated as the difference between the piston position at the end of the experiment and the piston position at the beginning of electroosmosis application, while for the samples treated with both processes, compression was calculated as the difference between the piston position after electroosmosis (end of experiment) and the piston position at the time of delivery of the first electroporation pulse.

In general, the highest compression values were obtained when samples were treated with both processes. However, it can be observed that samples in which the polarity was in Configuration B have, on average, higher compression. This is due to the fact that the liquid inside the sample moves towards the cathode, which in configuration B is the bottom electrode. When the cathode is the top electrode (conf. A), the flow exerts a force that opposes the compression force, resulting in lower compression values than in the case of polarity configuration B, where the cathode is the bottom electrode.

In cases where only electroosmosis is used, the compression values are slightly higher when polarity is maintained in configuration A, but the difference is so small as to be for all intents and purposes, negligible.

In the cases where both PEF and electroosmosis are applied, the standard deviation is higher than in the clusters where the processes are analysed individually, since several variables are involved. To reduce the standard deviation, the experiments would have to be repeated and many more samples analysed.

Statistical significance of the found differences was also analysed here, and p-values were calculated for different combinations, which are reported in Table 4.

| STATISTICAL ANALYSIS | | | | | |
|---|---|---|---|---|---|
| Variable 1 | Samples V1 | Variable 2 | Samples V2 | p-value | p-value < α |
| 900 V PEF - 10 V EOS - 10 N - Conf A | 10 | 900 V PEF - 10 V EOS - 10 N - Conf B | 10 | 0,001085234 | yes |
| 900 V PEF - 10 V EOS - 10 N - Conf A | 10 | 10 V EOS - 10 N - Conf A | 5 | 5,08539E-09 | yes |
| 900 V PEF - 10 V EOS - 10 N - Conf A | 10 | 10 V EOS - 10 N - Conf B | 5 | 2,39712E-10 | yes |
| 900 V PEF - 10 V EOS - 10 N - Conf A | 10 | 900 V PEF - 10 N | 5 | 1,66058E-06 | yes |
| 900 V PEF - 10 V EOS - 10 N - Conf B | 10 | 900 V PEF - 10 N | 5 | 4,07673E-08 | yes |
| 10 V EOS - 10 N - Conf A | 5 | 900 V PEF - 10 N | 5 | 3,10804E-06 | yes |
| 10 V EOS - 10 N - Conf B | 5 | 900 V PEF - 10 N | 5 | 6,15014E-07 | yes |

Table 4: the samples analysed and the number of samples subjected to the t-test are reported for each line.

The table shows that all calculated p-values are below the threshold value of 0.05, so that the studied groups are statistically significally different, and significant in terms of the total compression achieved at the end of the processes.



Figure 26: Mean and standard deviation of clusters treated with electroporation and electroosmosis following electroporation considering increasing time intervals

Next, the mean and standard deviation of the compression values were calculated in the cases of pure electroporation and electroosmosis after electroporation. In Figure 26, compression was evaluated by considering the difference of compression in increasing time intervals 30 s apart, taking the compression value at the time of electroosmosis as reference in the case where both procedures are applied, while in the cluster where electroporation is applied, the compression value at the time of release of the first pulse was taken as reference.

The curves obtained for the clusters treated with the two generators show, on average, higher compression values. The slope of the first section shows that the effect of electroosmotic flow after electroporation greatly increases the compression value because

the fluids inside the cells can move more freely after rupture of the cell membranes, which increases the sample compressibility. However, when the space available for the fluid is saturated, the slope of the curve tends to decrease. Eventually, were the experiments run for a longer time, a plateau would have been reached as the void space would be completely exhausted and thus maximum compression achieved. Again, the standard deviation values are high due to the biological origin of the tissue samples, however, this could be decreased further by increasing the number of analysed samples.

The statistically significant difference of the various groups relative to the compression values in the incremental time instants in Figure 26 was then analysed and is presented in the following table.

| STATISTICAL ANALYSIS | | | | | | |
|---|---|---|---|---|---|---|
| Interval | Variable 1 | Samples V1 | Variable 2 | Samples V2 | p-value | p-value < α |
| EOS - PEF | 900 V PEF - 10 V EOS - 10 N - Conf A | 10 | 900 V PEF - 10 V EOS - 10 N - Conf B | 10 | 0,786956013 | no |
| (EOS + 30s) - EOS | 900 V PEF - 10 V EOS - 10 N - Conf A | 10 | 900 V PEF - 10 V EOS - 10 N - Conf B | 10 | 0,490198102 | no |
| (EOS + 60s) - EOS | 900 V PEF - 10 V EOS - 10 N - Conf A | 10 | 900 V PEF - 10 V EOS - 10 N - Conf B | 10 | 0,417203595 | no |
| (EOS + 90s) - EOS | 900 V PEF - 10 V EOS - 10 N - Conf A | 10 | 900 V PEF - 10 V EOS - 10 N - Conf B | 10 | 0,251716189 | yes |
| (EOS + 120s) - EOS | 900 V PEF - 10 V EOS - 10 N - Conf A | 10 | 900 V PEF - 10 V EOS - 10 N - Conf B | 10 | 0,135763586 | yes |
| (EOS + 150s) - EOS | 900 V PEF - 10 V EOS - 10 N - Conf A | 10 | 900 V PEF - 10 V EOS - 10 N - Conf B | 10 | 0,060973058 | yes |
| (EOS + 180s) - EOS | 900 V PEF - 10 V EOS - 10 N - Conf A | 10 | 900 V PEF - 10 V EOS - 10 N - Conf B | 10 | 0,023091178 | yes |
| (EOS + 210s) - EOS | 900 V PEF - 10 V EOS - 10 N - Conf A | 10 | 900 V PEF - 10 V EOS - 10 N - Conf B | 10 | 0,011436446 | yes |
| (EOS + 240s) - EOS | 900 V PEF - 10 V EOS - 10 N - Conf A | 10 | 900 V PEF - 10 V EOS - 10 N - Conf B | 10 | 0,006276199 | yes |
| EOS - PEF | 900 V PEF - 10 V EOS - 10 N - Conf A | 10 | 900 V PEF - 10 N | 5 | 3,42616E-06 | yes |
| (EOS + 30s) - EOS | 900 V PEF - 10 V EOS - 10 N - Conf A | 10 | 900 V PEF - 10 N | 5 | 0,001021379 | yes |
| (EOS + 60s) - EOS | 900 V PEF - 10 V EOS - 10 N - Conf A | 10 | 900 V PEF - 10 N | 5 | 5,46486E-05 | yes |
| (EOS + 90s) - EOS | 900 V PEF - 10 V EOS - 10 N - Conf A | 10 | 900 V PEF - 10 N | 5 | 1,16179E-05 | yes |
| (EOS + 120s) - EOS | 900 V PEF - 10 V EOS - 10 N - Conf A | 10 | 900 V PEF - 10 N | 5 | 5,64076E-06 | yes |
| (EOS + 150s) - EOS | 900 V PEF - 10 V EOS - 10 N - Conf A | 10 | 900 V PEF - 10 N | 5 | 4,05893E-06 | yes |
| (EOS + 180s) - EOS | 900 V PEF - 10 V EOS - 10 N - Conf A | 10 | 900 V PEF - 10 N | 5 | 3,53844E-06 | yes |
| (EOS + 210s) - EOS | 900 V PEF - 10 V EOS - 10 N - Conf A | 10 | 900 V PEF - 10 N | 5 | 3,48912E-06 | yes |
| (EOS + 240s) - EOS | 900 V PEF - 10 V EOS - 10 N - Conf A | 10 | 900 V PEF - 10 N | 5 | 2,9869E-06 | yes |
| EOS - PEF | 900 V PEF - 10 V EOS - 10 N - Conf B | 10 | 900 V PEF - 10 N | 5 | 0,000118342 | yes |
| (EOS + 30s) - EOS | 900 V PEF - 10 V EOS - 10 N - Conf B | 10 | 900 V PEF - 10 N | 5 | 0,058920791 | yes |
| (EOS + 60s) - EOS | 900 V PEF - 10 V EOS - 10 N - Conf B | 10 | 900 V PEF - 10 N | 5 | 0,017183532 | yes |
| (EOS + 90s) - EOS | 900 V PEF - 10 V EOS - 10 N - Conf B | 10 | 900 V PEF - 10 N | 5 | 0,004564224 | yes |
| (EOS + 120s) - EOS | 900 V PEF - 10 V EOS - 10 N - Conf B | 10 | 900 V PEF - 10 N | 5 | 0,00145983 | yes |
| (EOS + 150s) - EOS | 900 V PEF - 10 V EOS - 10 N - Conf B | 10 | 900 V PEF - 10 N | 5 | 0,000458552 | yes |
| (EOS + 180s) - EOS | 900 V PEF - 10 V EOS - 10 N - Conf B | 10 | 900 V PEF - 10 N | 5 | 0,000129875 | yes |
| (EOS + 210s) - EOS | 900 V PEF - 10 V EOS - 10 N - Conf B | 10 | 900 V PEF - 10 N | 5 | 5,48151E-05 | yes |
| (EOS + 240s) - EOS | 900 V PEF - 10 V EOS - 10 N - Conf B | 10 | 900 V PEF - 10 N | 5 | 3,02548E-05 | yes |

Table 5: the samples analysed and the number of samples subjected to the t-test are reported for each line.

Table 5 highlights p-values that are higher than 0.05 only when comparing the group treated with both generators and polarity configuration A with the group treated with both generators and polarity configuration B. However, these values are higher from the initial moment up to 150 s after the application of electroporation. In contrast, in the time intervals

exceeding 150 s, p-values are obtained that demonstrate a statistically significant difference between the two groups.



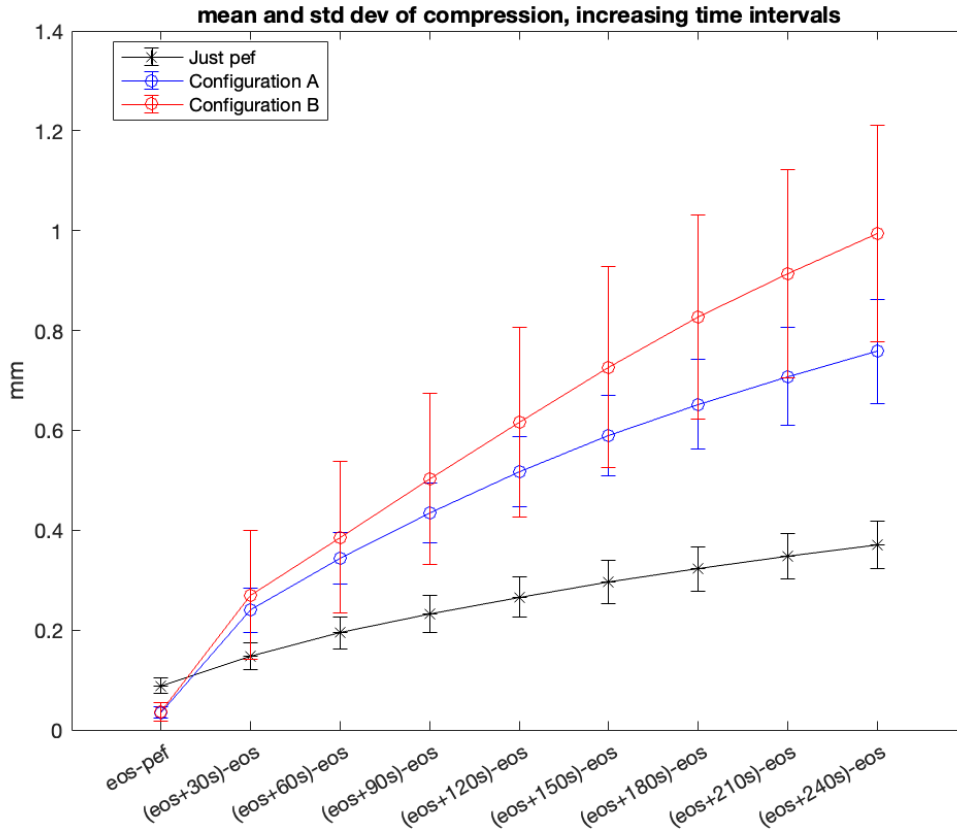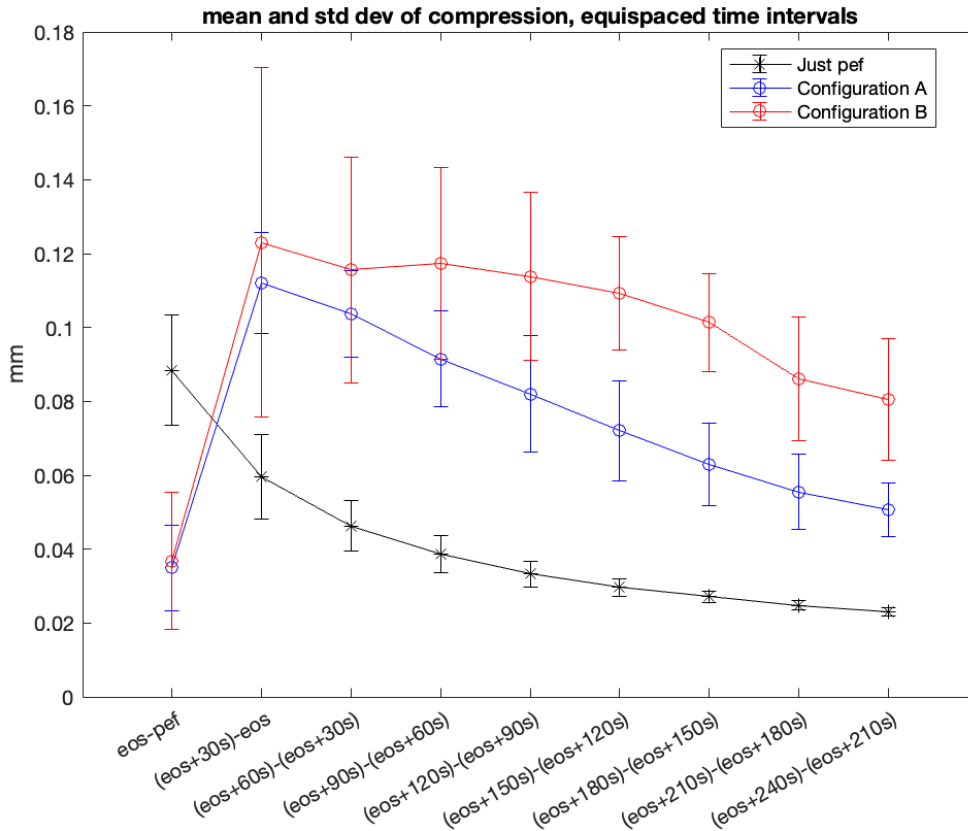Figure 27: Mean and standard deviation of clusters treated with electroporation and electroosmosis following electroporation considering equidistantly spaced time intervals.

Figure 27 shows similar curves to the previous case, but in this case the time intervals are equidistant. Each interval where the difference of the compression values is considered is 30 s. Thus, this graph shows the evolution of compression with increasing time. As can be seen above, the distance where the largest increase occurs is the initial distance, after which the compression values are always positive, but tend to decrease as time progresses. If the experiment is performed with a longer run time, the trend of the curves tends to reach a constant compression value.

The same analysis regarding statistically significant differences between the groups was performed, however, now considering equidistantly spaced time intervals. Table 6 shows the results of statistical analysis.

| | | | STATISTICAL ANALYSIS | | | |
|---|---|---|---|---|---|---|
| Intervals | Variable 1 | Samples V1 | Variable 2 | Samples V2 | p-value | p-value < α |
| EOS - PEF | 900 V PEF - 10 V EOS - 10 N - Conf A | 10 | 900 V PEF - 10 V EOS - 10 N - Conf B | 10 | 0,786956013 | no |
| (EOS + 30 s) - EOS | 900 V PEF - 10 V EOS - 10 N - Conf A | 10 | 900 V PEF - 10 V EOS - 10 N - Conf B | 10 | 0,487902772 | no |
| (EOS + 60 s) - (EOS + 30 s) | 900 V PEF - 10 V EOS - 10 N - Conf A | 10 | 900 V PEF - 10 V EOS - 10 N - Conf B | 10 | 0,261882815 | no |
| (EOS + 90 s) - (EOS + 60 s) | 900 V PEF - 10 V EOS - 10 N - Conf A | 10 | 900 V PEF - 10 V EOS - 10 N - Conf B | 10 | 0,011613776 | yes |
| (EOS + 120 s) - (EOS + 90 s) | 900 V PEF - 10 V EOS - 10 N - Conf A | 10 | 900 V PEF - 10 V EOS - 10 N - Conf B | 10 | 0,00190199 | yes |
| (EOS + 150 s) - (EOS + 120 s) | 900 V PEF - 10 V EOS - 10 N - Conf A | 10 | 900 V PEF - 10 V EOS - 10 N - Conf B | 10 | 1,94468E-05 | yes |
| (EOS + 180 s) - (EOS + 150 s) | 900 V PEF - 10 V EOS - 10 N - Conf A | 10 | 900 V PEF - 10 V EOS - 10 N - Conf B | 10 | 1,67676E-06 | yes |
| (EOS + 210 s) - (EOS + 180 s) | 900 V PEF - 10 V EOS - 10 N - Conf A | 10 | 900 V PEF - 10 V EOS - 10 N - Conf B | 10 | 0,00010437 | yes |
| (EOS + 240 s) - (EOS + 210 s) | 900 V PEF - 10 V EOS - 10 N - Conf A | 10 | 900 V PEF - 10 V EOS - 10 N - Conf B | 10 | 5,33809E-05 | yes |
| EOS - PEF | 900 V PEF - 10 V EOS - 10 N - Conf A | 10 | 900 V PEF - 10 N | 5 | 3,42616E-06 | yes |
| (EOS + 30 s) - EOS | 900 V PEF - 10 V EOS - 10 N - Conf A | 10 | 900 V PEF - 10 N | 5 | 5,72093E-06 | yes |
| (EOS + 60 s) - (EOS + 30 s) | 900 V PEF - 10 V EOS - 10 N - Conf A | 10 | 900 V PEF - 10 N | 5 | 1,76084E-07 | yes |
| (EOS + 90 s) - (EOS + 60 s) | 900 V PEF - 10 V EOS - 10 N - Conf A | 10 | 900 V PEF - 10 N | 5 | 9,47181E-07 | yes |
| (EOS + 120 s) - (EOS + 90 s) | 900 V PEF - 10 V EOS - 10 N - Conf A | 10 | 900 V PEF - 10 N | 5 | 1,399E-05 | yes |
| (EOS + 150 s) - (EOS + 120 s) | 900 V PEF - 10 V EOS - 10 N - Conf A | 10 | 900 V PEF - 10 N | 5 | 1,15434E-05 | yes |
| (EOS + 180 s) - (EOS + 150 s) | 900 V PEF - 10 V EOS - 10 N - Conf A | 10 | 900 V PEF - 10 N | 5 | 9,28836E-06 | yes |
| (EOS + 210 s) - (EOS + 180 s) | 900 V PEF - 10 V EOS - 10 N - Conf A | 10 | 900 V PEF - 10 N | 5 | 1,57956E-05 | yes |
| (EOS + 240 s) - (EOS + 210 s) | 900 V PEF - 10 V EOS - 10 N - Conf A | 10 | 900 V PEF - 10 N | 5 | 1,33014E-06 | yes |
| EOS - PEF | 900 V PEF - 10 V EOS - 10 N - Conf B | 10 | 900 V PEF - 10 N | 5 | 0,000118342 | yes |
| (EOS + 30 s) - EOS | 900 V PEF - 10 V EOS - 10 N - Conf B | 10 | 900 V PEF - 10 N | 5 | 0,01227314 | yes |
| (EOS + 60 s) - (EOS + 30 s) | 900 V PEF - 10 V EOS - 10 N - Conf B | 10 | 900 V PEF - 10 N | 5 | 0,000269469 | yes |
| (EOS + 90 s) - (EOS + 60 s) | 900 V PEF - 10 V EOS - 10 N - Conf B | 10 | 900 V PEF - 10 N | 5 | 1,73614E-05 | yes |
| (EOS + 120 s) - (EOS + 90 s) | 900 V PEF - 10 V EOS - 10 N - Conf B | 10 | 900 V PEF - 10 N | 5 | 3,23416E-06 | yes |
| (EOS + 150 s) - (EOS + 120 s) | 900 V PEF - 10 V EOS - 10 N - Conf B | 10 | 900 V PEF - 10 N | 5 | 4,25375E-08 | yes |
| (EOS + 180 s) - (EOS + 150 s) | 900 V PEF - 10 V EOS - 10 N - Conf B | 10 | 900 V PEF - 10 N | 5 | 1,79048E-08 | yes |
| (EOS + 210 s) - (EOS + 180 s) | 900 V PEF - 10 V EOS - 10 N - Conf B | 10 | 900 V PEF - 10 N | 5 | 2,21905E-06 | yes |
| (EOS + 240 s) - (EOS + 210 s) | 900 V PEF - 10 V EOS - 10 N - Conf B | 10 | 900 V PEF - 10 N | 5 | 3,51447E-06 | yes |

Table 6: the samples analysed and the number of samples subjected to the t-test are reported for each line.

In samples where compression differences between equally spaced time intervals are considered, the p-values obtained are always less than 0.05, except when comparing groups treated with both generators but with different polarity configurations. In this case, the p-values for the first three intervals are greater than 0.05, but with a decreasing tendency with each successive interval.

The significance of data presented in Figure 26 and Figure 27 is that compression kinetics of tissue samples are dramatically affected by inducing of an additional electroosmotic flow post-electroporation (post-pulse) application, while this flow is practically insignificant if there is no electroporation application (as demonstrated by the 10 samples shown in Figure 23). Moreover, the degree to which tissue is compressed by the superimposed electroosmotic flow is dependent on the configuration of polarity of the electrodes. This means our initial assumptions were correct, that our understanding of (plant) tissue electroporation is basically sound and follows the following narration.

Raw, turgid, fresh plant tissue, high in conductive liquid predominantly found within the cells (as opposed to in the extracellular space), is affected by the electroporation pulses that disrupt the selective permeability of the cell membrane. As a result, cells no longer control efflux of liquid from within their interior, and turgor pressure is significantly reduced in the affected cells. Liquid, now spewing out of the cells into the extracellular space, is to a

degree subject to forced transport by electroosmosis during subsequent (after the very first pulse that causes electroporation of tissue) pulses. The direction of this flow depends on the electrode configuration in the sense of electrode polarity, whereby liquid will tend to move towards the cathode due to electroosmosis.

# Chapter 4

# Conclusions

## 4. Conclusions

The objective of this thesis was to observe and evaluate mass transport phenomena resulting from the electroosmotic flow during electroporation. These mass transport phenomena were studied using two different protocols:

1. The first part of the project was carried out with the aim of evaluating the mass transport phenomena resulting from the electroosmotic effect when pulsed electric fields are applied to both plant and animal tissues. For this purpose, it was necessary to collect data from the plant tissue samples subjected to the different experimental protocols using a texture analyser and an oscilloscope. The data from animal tissues were previously collected in experiments performed by Genovese et al. in the same laboratory using the very same procedures as for the plant tissue samples. The results of the experiments performed according to the first protocol showed that there is indeed a detectable, but small contribution of the electroosmotic flow during the electroporation process itself, mainly due to rather short pulses being used for achieving tissue electroporation (on the order of 100s of μs). This small contribution to mass transport due to electroosmotic flow occurs both in animal tissue as well as in plant tissue, where it is perhaps just as significant as in animal tissue, but can be harder to detect using the method of texture analysis due to the massive releases in turgor pressure that occur when turgid plant tissue is electroporated. Because animal tissue does not have a cell wall among its structural components, it exhibits a more regular pattern than plant tissue, which does have a cell wall and exhibits significant turgidity. Using the data from the plant tissue, a comparison was also made between different parameters, such as external

compression force and electrode polarity configuration, but the differences were found not to be statistically significant using a t-test.

2. On the other hand, the second part of the project was carried out to evaluate the mass transport phenomenon of electroosmosis induced in the plant tissue after the application of pulsed electric fields using a LV generator applying constant direct current. Compression behaviour of samples treated with both generators was compared to behaviour of samples treated only with the HV generator and with samples treated only with the LV generator, and in general the effects of electroosmotic flow were demonstrated to be significantly higher when the electroosmotic flow is preceded by the application of electroporation.

In conclusion, the contribution of electroosmosis to mass transport during the electroporation process in plant-based tissues has been clearly evidenced through the work presented in this thesis, a result of significance to the food processing field of research. A scientific publication detailing the work will be prepared and submitted to a suitable journal following the completion of this thesis. The results have implications for the biomedical field as well, since electroosmosis was found to be detectable by the used method in animal tissues as well, but further work is necessary in this field before significant conclusions can be drawn and published about, especially since all the animal tissue samples analysed within the scope of this work have been obtained *ex vivo* several hours *post mortem*.

Future research work will focus on consolidating the findings obtained on plant tissue, generalising them, and attempting to translate the findings onto animal tissues and consequently determining the degree of significance of obtained results for biomedical applications of electroporation, perhaps through not only experimental work, but also numerical modelling. It is envisioned that the dual porosity model could be further enhanced and upgraded with electroosmosis as an important mass transport mechanism, once the phenomenon is fully characterised and well researched in animal tissues as well as it is now in tissues of plant origin.

# Bibliography

ANDRÉ, F. M., GEHL, J., SERSA, G., ET AL. 2008. Efficiency of High- and Low-Voltage Pulse Combinations for Gene Electrotransfer in Muscle, Liver, Tumor, and Skin. *Human Gene Therapy 19*, 11, 1261–1272.

CASAGRANDE, A. //. ELECTRO-OSMOTIC STABILIZATION OF SOILS. *Boston Society Civil Engineers Journal* 0.

CEMAZAR, M., GOLZIO, M., SERSA, G., ET AL. 2012. Hyaluronidase and Collagenase Increase the Transfection Efficiency of Gene Electrotransfer in Various Murine Tumors. *Human Gene Therapy 23*, 1, 128–137.

DAVALOS, R.V., MIR, I.L.M., AND RUBINSKY, B. 2005. Tissue ablation with irreversible electroporation. *Annals of Biomedical Engineering 33*, 2, 223–231.

DYMEK, K. 2015. Modeling electroporation of the non-treated and vacuum impregnated heterogeneous tissue of spinach leaves. 10.

EDD, J.F., HOROWITZ, L., DAVALOS, R.V., MIR, L.M., AND RUBINSKY, B. 2006. In vivo results of a new focal tissue ablation technique: irreversible electroporation. *IEEE Transactions on Biomedical Engineering 53*, 7, 1409–1415.

FARAJI, A.H., JAQUINS-GERSTL, A.S., VALENTA, A.C., OU, Y., AND WEBER, S.G. 2020. Electrokinetic Convection-Enhanced Delivery of Solutes to the Brain. *ACS Chemical Neuroscience 11*, 14, 2085–2093.

GEBOERS, B., SCHEFFER, H.J., GRAYBILL, P.M., ET AL. 2020. High-Voltage Electrical Pulses in Oncology: Irreversible Electroporation, Electrochemotherapy, Gene Electrotransfer, Electrofusion, and Electroimmunotherapy. *295*, 2, 19.

GENOVESE, J., KRANJC, M., SERŠA, I., ET AL. 2021. PEF-treated plant and animal tissues: Insights by approaching with different electroporation assessment methods. *Innovative Food Science & Emerging Technologies 74*, 102872.

GENOVESE, J., STRUČIĆ, M., SERŠA, I., ET AL. 2023. PEF treatment effect on plant tissues of heterogeneous structure no longer an enigma: MRI insights beyond the naked eye. *Food Chemistry 405*, 134892.

GRANOT, Y. AND RUBINSKY, B. 2008. Mass transfer model for drug delivery in tissue cells with reversible electroporation. *International Journal of Heat and Mass Transfer 51*, 23, 5610–5616.

GRAY, D.H. AND MITCHELL, J.K. 1967. Fundamental Aspects of Electro-Osmosis in Soils. *Journal of the Soil Mechanics and Foundations Division 93*, 6, 209–236.

HARGRAVE, B., JR, R.S., NAVARE, S., ET AL. 2014. Gene Electro Transfer of Plasmid Encoding Vascular Endothelial Growth Factor for Enhanced Expression and Perfusion in the Ischemic Swine Heart. *PLOS ONE 9*, 12, e115235.

HELLER, R. AND HELLER, L.C. 2015. Chapter Eight - Gene Electrotransfer Clinical Trials. In: L. Huang, D. Liu and E. Wagner, eds., *Advances in Genetics*. Academic Press, 235–262.

HOFMANN, G.A., DEV, S.B., DIMMER, S., AND NANDA, G.S. 1999. Electroporation therapy: a new approach for the treatment of head and neck cancer. *IEEE transactions on bio-medical engineering 46*, 6, 752–759.

HUO, Z.-Y., WINTER, L.R., WANG, X.-X., ET AL. 2022. Synergistic Nanowire-Enhanced Electroporation and Electrochlorination for Highly Efficient Water Disinfection. *Environmental Science & Technology 56*, 15, 10925–10934.

IWATA, M., IGAMI, H., MURASE, T., AND YOSHIDA, H. 1991. Analysis of Electroosmotic Dewatering. *Journal of Chemical Engineering of Japan 24*, 1, 45–50.

KLEIN, N., GUENTHER, E., MIKUS, P., STEHLING, M.K., AND RUBINSKY, B. 2017. Single exponential decay waveform; a synergistic combination of electroporation and electrolysis (E2) for tissue ablation. *PeerJ 5*, e3190.

KLEIN, N., MERCADAL, B., STEHLING, M., AND IVORRA, A. 2020. In vitro study on the mechanisms of action of electrolytic electroporation (E2). *Bioelectrochemistry (Amsterdam, Netherlands) 133*, 107482.

KOTNIK, T., FREY, W., SACK, M., HABERL MEGLIČ, S., PETERKA, M., AND MIKLAVČIČ, D. 2015. Electroporation-based applications in biotechnology. *Trends in Biotechnology 33*, 8, 480–488.

KOTNIK, T., REMS, L., TAREK, M., AND MIKLAVČIČ, D. 2019. Membrane Electroporation and Electropermeabilization: Mechanisms and Models. *Annual Review of Biophysics 48*, 1, 63–91.

LANOISELLÉ, J.-L., VOROBYOV, E.I., BOUVIER, J.-M., AND PAIR, G. 1996. Modeling of solid/liquid expression for cellular materials. *AIChE Journal 42*, 7, 2057–2068.

MAHNIČ-KALAMIZA, S., MIKLAVČIČ, D., AND VOROBIEV, E. 2015. Dual-porosity model of mass transport in electroporated biological tissue: Simulations and experimental work for model validation. *Innovative Food Science & Emerging Technologies 29*, 41–54.

MAHNIČ-KALAMIZA, S. AND VOROBIEV, E. 2014. Dual-porosity model of liquid extraction by pressing from biological tissue modified by electroporation. *Journal of Food Engineering 137*, 76–87.

MAHNIČ-KALAMIZA, S., VOROBIEV, E., AND MIKLAVČIČ, D. 2014. Electroporation in Food Processing and Biorefinery. *The Journal of Membrane Biology 247*, 12, 1279–1304.

MARTY, M., SERSA, G., GARBAY, J.R., ET AL. 2006. Electrochemotherapy – An easy, highly effective and safe treatment of cutaneous and subcutaneous metastases: Results of ESOPE (European Standard Operating Procedures of Electrochemotherapy) study. *European Journal of Cancer Supplements 4*, 11, 3–13.

MENON, A., MASHYAMOMBE, T.R., KAYGEN, E., MORTAZAVI NASIRI, M.S., AND STOJCESKA, V. 2019. Electro-osmosis dewatering as an energy efficient technique for drying food materials. *Energy Procedia 161*, 123–132.

MERRILL, D.R., BIKSON, M., AND JEFFERYS, J.G.R. 2005. Electrical stimulation of excitable tissue: design of efficacious and safe protocols. *Journal of Neuroscience Methods 141*, 2, 171–198.

MIKLAVČIČ, D., MALI, B., KOS, B., HELLER, R., AND SERŠA, G. 2014. Electrochemotherapy: from the drawing board into medical practice. *Biomedical Engineering Online 13*, 1, 29.

MORAGA, G., MARTÍNEZ-NAVARRETE, N., AND CHIRALT, A. 2006. Compositional Changes of Strawberry Due to Dehydration, Cold Storage and Freezing–Thawing Processes. *Journal of Food Processing and Preservation 30*, 4, 458–474.

NEUMANN, E., SCHAEFER-RIDDER, M., WANG, Y., AND HOFSCHNEIDER, P.H. 1982. Gene transfer into mouse lyoma cells by electroporation in high electric fields. *The EMBO Journal 1*, 7, 841–845.

OKINO, M. AND MOHRI, H. 1987. Effects of a high-voltage electrical impulse and an anticancer drug on in vivo growing tumors. *Japanese Journal of Cancer Research: Gann 78*, 12, 1319–1321.

PARNIAKOV, O., BARBA, F.J., GRIMI, N., LEBOVKA, N., AND VOROBIEV, E. 2016. Extraction assisted by pulsed electric energy as a potential tool for green and sustainable recovery of nutritionally valuable compounds from mango peels. *Food Chemistry 192*, 842–848.

PATARO, G., FALCONE, M., DONSÌ, G., AND FERRARI, G. 2014. Metal release from stainless steel electrodes of a PEF treatment chamber: Effects of electrical parameters and food composition. *Innovative Food Science & Emerging Technologies 21*, 58–65.

SACK, M., EING, C., BERGHOFE, T., ET AL. 2008. Electroporation-Assisted Dewatering as an Alternative Method for Drying Plants. *IEEE Transactions on Plasma Science 36*, 5, 2577–2585.

SERSA, G., MIKLAVCIC, D., CEMAZAR, M., RUDOLF, Z., PUCIHAR, G., AND SNOJ, M. 2008. Electrochemotherapy in treatment of tumours. *European Journal of Surgical Oncology (EJSO) 34*, 2, 232–240.

TREZISE, A.E.O. 2002. In Vivo DNA Electrotransfer. *DNA and Cell Biology 21*, 12, 869–877.

VELICKOVA, E., TYLEWICZ, U., DALLA ROSA, M., WINKELHAUSEN, E., KUZMANOVA, S., AND GÓMEZ GALINDO, F. 2013. Effect of vacuum infused cryoprotectants on the freezing tolerance of strawberry tissues. *LWT - Food Science and Technology 52*, 2, 146–150.

VIJH, A. 2004. Electrochemical treatment (ECT) of cancerous tumours: necrosis involving hydrogen cavitation, chlorine bleaching, pH changes, electroosmosis. *International Journal of Hydrogen Energy 29*, 6, 663–665.

VIJH, A.K. 1999a. Electrochemical Treatment of Tumors (ect): Electroosmotic Dewatering (eod) as the Primary Mechanism. *Drying Technology 17*, 3, 586–596.

VIJH, A.K. 1999b. Electrochemical field effects in biological materials: electro-osmotic dewatering of cancerous tissue as the mechanistic proposal for the electrochemical treatment of tumors. *Journal of Materials Science. Materials in Medicine 10*, 7, 419–423.

# Ringraziamenti

Questo lungo ed impegnativo percorso universitario è giunto (finalmente) al termine. Voglio ringraziare la mia famiglia, i miei amici, e chiunque abbia contribuito, seppur in minima parte, al raggiungimento di questo tanto bramato obiettivo.

Vorrei aggiungere inoltre dei ringraziamenti speciali.

In primis vorrei ringraziare mamma e papà, per i sacrifici che hanno fatto per consentirmi di arrivare fino ad oggi, per aver fatto 600km in una notte ed aver dormito in una macchina con -3 °C in un parcheggio sloveno. Grazie davvero, siete l'esempio perfetto di genitore che un giorno vorrei essere.

Vorrei inoltre ringraziare i miei fratelli Alessio ed Elena, "separati" dalla distanza ma comunque inseparabili compagni di avventure. Siete i migliori amici che ho da sempre e che mi hanno sempre sostenuto.

Un altro ringraziamento va a mio fratello per scelta, Andrea, per essere la spalla su cui contare sempre e da sempre, non che compagno di padel eccezionale.

Ringrazio l'ultimo fratello (siamo una famiglia numerosa) ritrovato dopo tanti anni, Francesco, nuovo gymbro ma anche un vero amico su cui contare.

Infine, l'ultimo ringraziamento va alla mia ragazza Alessia, supporto fondamentale che mi ha spronato sempre a dare il meglio di me.

Nonostante sia stato difficile, siamo arrivati alla fine, tutti insieme, e adesso siamo pronti per un nuovo capitolo.

Ggez.